INSTITUTO SUPERIOR DE ENGENHARIA DE LISBOA

Área Departamental de Engenharia Eletrónica e Telecomunicações e de Computadores

LEDs assisted navigation in connected cars

MIRTES ALAÍSE MARTINS DE LIMA
(Licenciada em Engenharia Eletrónica e Telecomunicações e de Computadores)

Dissertação de natureza científica para obtenção do grau de Mestre em Engenharia Eletrónica e Telecomunicações

Orientadoras:
Prof. Doutora Paula Maria Garcia Louro
Prof. Doutora Maria Manuela Almeida Carvalho Vieira

Júri:
Presidente: Prof. Doutor António João Nunes Serrador
Vogais:
Prof. Doutor Pedro Manuel de Almeida Carvalho Vieira
Prof. Doutora Paula Maria Garcia Louro

Março de 2022

INSTITUTO SUPERIOR DE ENGENHARIA DE LISBOA

Área Departamental de Engenharia Eletrónica e Telecomunicações e de Computadores

LEDs assisted navigation in connected cars

MIRTES ALAÍSE MARTINS DE LIMA
(Licenciada em Engenharia Eletrónica e Telecomunicações e de Computadores)

Dissertação de natureza científica para obtenção do grau de Mestre em Engenharia Eletrónica e Telecomunicações

Orientadoras:
Prof. Doutora Paula Maria Garcia Louro
Prof. Doutora Maria Manuela Almeida Carvalho Vieira

Júri:
Presidente: Prof. Doutor António João Nunes Serrador
Vogais:
Prof. Doutor Pedro Manuel de Almeida Carvalho Vieira
Prof. Doutora Paula Maria Garcia Louro

Março de 2022

Acknowledgement

To my loving and caring parents José de Lima and Maria da Graça de Lima, who have done everything in their power to make sure I would become the best version of myself. Thank you for your love and support, thank you for working hard to provide the best education, thank you for always believing in me and making sure I knew that. Everything I am and have today is because of your efforts. I love both of you from the bottom of my hearth and wish to be even if a fraction of what you are. It is a pleasure to be your daughter and my greatest accomplishment in life is to make you proud and happy.

To my sister Elaine and my brother Igor for being such great siblings and role models to me. I love both of you and it is an honor being your little sister. And to all my family who have helped me in any way throughout my life.

A special thank you to my mentors and supervisors Dr. Paula Louro and Dr. Manuela Vieira for guiding me this past year. Thank you for your effort in making sure this would turn out the best work possible and thank you for showing me a different side of engineering that I didn't know I would like so much. And to Dr. Pedro Vieira for presenting me this dissertation.

I would also like to extend my appreciation to the teachers who in any way taught me valuable lesson in school and in life. And my friends, especially the ones I met in Lisbon. Thank you for showing me a different side of life and for brightening my days.

Finally, to Instituto Superior de Engenharia de Lisboa for accepting and welcoming me and for the opportunity to learn so much with the best teachers. All that I learn here I will put to use and become the best engineer possible.

To project IPL/IDICA/2020/Geo_Loc/ISEL for the opportunity and resources to develop this dissertation.

Abstract

Alternative wireless technologies are needed due to the increasing traffic demand and the shortage of RF band. VLC uses the visible light spectrum to encode and transmit information and is a complement to RF, providing additional bandwidth.

Traffic lights are the main infrastructures to control access to roads and will soon be replaced by more efficient structures to improve traffic management.

The goal of this dissertation is the characterization and test of communication links based on VLC technology for road management applications.

Transmitters of the VLC link are tetrachromatic white LEDs used for illumination and data transmission. The characterization of the optical transmitter system is done through MATLAB simulations, using the Lambertian model. Receivers based on a-SiC:H/a-Si:H photodiodes with selective spectral sensitivity are used to.

The studied scenario is a crossroad formed by five cells, with a LED at each corner providing a certain coverage and forming nine footprints. The OOK modulation was used, and the transmitted message follows a 64-bit frame structure.

The coverage map and footprint map were obtained as outputs. A calibration curve was used in the encoding and decoding process.

Two trajectories were tested: vehicle moving from West to East and from West to North. The encoded process was successful, proving that the simulation tool developed produces valid results.

The decoding process was successful with the simulated results but not so much with the signals measured in the laboratory. The red LED/channel presented the least error followed by the green, since these are more distinguishable. The blue and violet LED/channel are less distinguishable and presented the most errors. Adjusting the calibration curve or implementing error detection mechanism are proposed as solutions.

A GUI was developed to enable easy interaction between the user and the simulation tool.

Keywords: VLC, connected vehicles, LED, Lambertian model, channel gain, decoding.

Resumo

Devido ao aumento da procura de tráfego e diminuição da banda RF disponível são necessárias tecnologias sem fios alternativas. O VLC utiliza o espetro visível para codificar e transmitir informação, sendo um complemento ao RF fornecendo largura de banda adicional.

Os semáforos são as principais infraestruturas de controlo de acesso às estradas e serão eventualmente substituídas por estruturas mais eficiente para melhorar a gestão do trânsito.

O objetivo desta dissertação é a caracterização e teste da comunicação utilizando a tecnologia VLC em aplicações de gestão rodoviária.

Os transmissores usados para iluminação e comunicação são LEDs tetra-cromáticos. A caracterização do transmissor ótico foi realizada em MATLAB usando o modelo Lambertiano. O recetor utilizado é um foto-detetor baseado em estruturas pin de a-SiC:H e a-Si:H que apresentam sensibilidade espectral seletiva.

O cenário estudado é um cruzamento formado por cinco células, com um LED em cada canto, proporcionando uma cobertura específica e formando em conjunto nove *footprints*. Foi usada a modulação OOK e a mensagem enviada utiliza uma estrutura de 64 bits.

Como resultados, foram obtidos mapas de cobertura e de *footprints*. A curva de calibração foi usada para o processo de codificação e descodificação.

Foram testadas duas trajetórias: veículos provenientes de Oeste para Este e de Oeste para Norte. O processo de codificação foi bem-sucedido, mostrando que a ferramenta de simulação desenvolvida produz resultados válidos.

O processo de descodificação foi bem-sucedido para os resultados simulados, mas apresenta erros para as medidas laboratoriais. O LED/canal vermelho apresentou menos erros, seguido do verde pois estes são mais distinguíveis. O azul e o violeta são menos distinguíveis, apresentando mais erros. As soluções propostas são ajustar a curva de calibração ou implementar de mecanismos de deteção de erros.

Foi desenvolvida uma interface gráfica para facilitar a interação entre utilizador e ferramenta de simulação.

Palavras-chave: VLC, veículos conectados, LED, modelo Lambertiano, ganho do canal, descodificação.

Table of Contents

Acknowledgement v
Abstract vii
Resumo ix
List of Figures xiii
List of Tables xvii
List of Acronyms xix
List of Symbols xxi
1 Introduction 1
1.1 Goals of the dissertation 1
1.2 Structure of the report 1
1.3 Dissertation output 2
2 State of the Art 5
2.1 VLC, Visible Light Communication 5
2.1.1 Equipment (transmitter and receiver) 5
2.1.2 Architecture 6
2.2 VLC in Connected Vehicles 7
2.2.1 Modes of communication 8
2.3 VLC Advantages 8
2.3.1 General VLC Advantages 8
2.3.2 Vehicular VLC Advantages 9
2.4 VLC Challenges 9
2.5 Channel Model and Propagation Characteristics 10
2.5.1 Luminous Flux 11
2.5.2 Received Flux 11
2.5.3 Path Loss 12
2.5.4 Multipath 13
2.6 Modulation 13
2.6.1 On-Off Keying (OOK) 13

2.6.2 Pulse Modulation Methods 14
2.6.3 Orthogonal Frequency Division Multiplexing (OFDM) 14
2.6.4 Color Shift Keying (CSK) 14
3 Proposed Test Scenario (Methodology) 17
3.1 Experimental results 19
3.2 Phasing Diagram 22
4 Description of the Simulation Model 25
4.1 Emitted Power 25
4.2 Path Loss 25
4.3 Gain 26
4.3.1 Antenna model 26
4.3.2 Lambertian model 27
4.4 Link Budget 28
4.5 Calibration Curve 28
4.6 Frame Format 28
5 Results and Discussion 31
5.1 Coverage map 31
5.2 Footprint Map 32
5.3 Calibration curve 33
5.4 Tested Scenarios 34
5.4.1 West to East (straight path) 36
5.4.2 West to North (left turn) 44
5.5 Decoding 51
5.5.1 Decoding the simulated signal 51
5.5.2 Decoding the measured signal 55
5.6 Graphical User Interface 59
6 Conclusion and Future Work 63
References 67

List of Figures

Figure 2.1: A block diagram showing various modulates of VLC transmitter and receiver [2]. 7
Figure 2.2: Relative position of transmitter and receiver in LOS settings [2]. 12
Figure 3.1: Illustration of the proposed I2V2V2I2V communication scenario: (a) generic model for cooperative vehicular communication. (b) Connected vehicle communication link [10]....17
Figure 3.2: Lighting plan and generated joint footprints in a crossroad (LED array = RGBV color spots) [10]. 18
Figure 3.3: Frame structure representation. (a) Codification used to drive the headlights of a vehicle in a request message from footprint #8. R3;2, G3;1, and V2;1 are the transmitted node packets, in a time slot. (b) Encoded message response of the controller to a vehicle located in the crossroad (#1, R3;4, G3;3, B2;4, and V2;3) [10]. 19
Figure 3.4: Normalized MUX data signals. The parity MUX signal is also superimposed to exemplify the bit error detection. On the top, the transmitted channels packets [R, G, B, V] and parity bits [PR, PG, PB] are depicted. (a) Calibrated cell. (b) Signals acquired by a receiver in positions #1, cell [$R_{3,2}$, $G_{3,3}$, $B_{2,2}$, $V_{2,3}$] [10].....20
Figure 3.5: Normalized MUX signals acquired by a receiver at the crossroad in positions #1, #2, #4, #6, or #8. On the top, the transmitted channels packets [R, G, B, V] are decoded [10]. 21
Figure 3.6: (a) Physical area, color poses and channelization. (b) Representation of a phasing diagram [11]. 22
Figure 4.1: Pose orientation [33].....29
Figure 5.1: Coverage map of one cell.....32
Figure 5.2: Footprint map of one cell. 33
Figure 5.3: Normalized calibration curve. (a) Simulated. (b) Obtained via lab measurements. 34
Figure 5.4: Proposed scenario.....35
Figure 5.5: Example of vehicle trajectories [11]. 35
Figure 5.6: Proposed scenario, vehicle moving from West to East. 36
Figure 5.7: Results of the proposed scenario, West to East, cell C2 (position 1), footprint #4: (a) transmitted signals by each channel, (b) simulation of the normalized received signal and (c) normalized experimental received signal.....37
Figure 5.8: Results of the proposed scenario, West to East, cell C3 (position 2), footprint #4: (a) transmitted signals by each channel, (b) simulation of the normalized received signal and (c) normalized experimental received signal.....39

Figure 5.9: Results of the proposed scenario, West to East, cell C3 (position 3), footprint #5: (a) transmitted signals by each channel, (b) simulation of the normalized received signal and (c) normalized experimental received signal. 40
Figure 5.10: Results of the proposed scenario, West to East, cell C3 (position 4), footprint #6: (a) transmitted signals by each channel, (b) simulation of the normalized received signal and (c) normalized experimental received signal. 42
Figure 5.11: Results of the proposed scenario, West to East, cell C4 (position 5), footprint #6: (a) transmitted signals by each channel, (b) simulation of the normalized received signal and (c) normalized experimental received signal. 43
Figure 5.12: Proposed scenario, vehicle moving from West to North. 44
Figure 5.13: Results of the proposed scenario, West to North, cell C2 (position 1), footprint #1: (a) transmitted signals by each channel, (b) normalized simulation of the received signal and (c) normalized experimental received signal. 45
Figure 5.14: Results of the proposed scenario, West to North, cell C2 (position 2), footprint #4: (a) transmitted signals by each channel, (b) normalized simulation of the received signal and (c) normalized experimental received signal. 46
Figure 5.15: Results of the proposed scenario, West to North, cell C3 (position 3), footprint #3: (a) transmitted signals by each channel, (b) normalized simulation of the received signal and (c) normalized experimental received signal. 47
Figure 5.16: Results of the proposed scenario, West to North, cell C3 (position 4), footprint #1: (a) transmitted signals by each channel, (b) normalized simulation of the received signal and (c) normalized experimental received signal. 49
Figure 5.17: Results of the proposed scenario, West to North, cell C1 (position 5), footprint #1: (a) transmitted signals by each channel, (b) normalized simulation of the received signal and (c) normalized experimental received signal. 50
Figure 5.18: Decoded simulated signal, West to North, cell C2 (position 1), footprint #1: (a) received signal, (b) expected decoding result and (c) obtained decoding result. 52
Figure 5.19: Decoded simulated signal, West to East, cell C2 (position 1), footprint #4: (a) received signal, (b) expected decoding result and (c) obtained decoding result. 53
Figure 5.20: Decoded simulated signal, West to East, cell C3 (position 3), footprint #5: (a) received signal, (b) expected decoding result and (c) obtained decoding result. 54
Figure 5.21: Decoded measured signal, West to North, cell C3 (position 4), footprint #1: (a) received signal, (b) expected decoding result and (c) obtained decoding result. 55
Figure 5.22: Decoded measured signal, West to North, cell C4 (position 5), footprint #6: (a) received signal, (b) expected decoding result and (c) obtained decoding result. 57
Figure 5.23: Decoded measured signal, West to North, cell C3 (position 3), footprint #3: (a) received signal, (b) expected decoding result and (c) obtained decoding result. 58

Figure 5.24: Graphical User Interface, tab one. 59
Figure 5.25: Graphical User Interface, tab two. 60
Figure 5.26: Graphical User Interface, tab three. 61

List of Tables

Table 2.1: Advantages and disadvantages of various modulations used in VLC [2] [9] [27]. .15
Table 4.1: Frame structure. 28
Table 5.1: Link budget input. 31

List of Acronyms

3GPP	3rd Generation Partnership Project
ACO-OFDM	Asymmetrically Clipped Optical OFDM
a-Si:H	Hydrogenated Amorphous Silicon
a-SiC:H	Hydrogenated Amorphous Silicon Carbide
BMP	Bit Map
CSK	Color Shift Keying
DC	Direct Current
DCO-OFDM	DC-biased Optical OFDM
DMT	Discrete Multitone
DSRC	Dedicated Short-Range Communication
E	East
EOF	End of File
FOV	Field of View
GPS	Global Positioning System
GUI	Graphical User Interface
I2V	Infrastructure to Vehicle
ID	Identification
IM	Intersection Manager
LED	Light Emitting Diode
LOS	Line-of-Sight
MIMO	Multiple Input Multiple Output
N	North
NLOS	Non-Line-of-Sight
NRZ	Non-Return-to-Zero
OFDM	Orthogonal Frequency-Division Multiplexing
OOK	On-Off Keying
PPM	Pulse Position Modulation
PWN	Pulse Width Modulation
RF	Radio Frequency
RGB	Red, Green, Blue
RGBV	Red, Green, Blue, Violet
S	South
SNR	Signal-to-Noise Ratio
TLED	Tri-LED

V2I	Vehicle to Infrastructure
V2V	Vehicle to Vehicle
V2X	Vehicle to Everything
VLC	Visible Light Communication
VLP	Visible Light Positioning
W	West

List of Symbols

A, A_r	Receiver/photodetector area	[m]
$A_{dB}^{"}$	Antenna radiation power pattern	[dB]
A_{max}	Maximum attenuation	[dB]
d, D, D_{t-r}	Distance between transmitter and receiver	[m]
F_R	Receiver luminous flux	[lm]
F_T	Transmitter luminous flux	[lm]
G	Channel gain	
G_E, G_R	Emitter and receiver gain, respectively	[dB]
$g_t(\theta)$	Luminous intensity distribution	[cd]
I_N	Luminous intensity	[cd]
I_0	Axial intensity	[cd]
$\mathbf{L}$	Total attenuation/pathloss	[dB]
L_{Atm}	Attenuation due to adverse atmospheric condition	[dB]
L_L	Luminous path loss	
L_{Obst}	Attenuation due to obstacles	[dB]
m	Order of Lambertian emission	
P	Power	[W]
P_E, P_R	Emitted and received power, respectively	[dBm]
$\mathbf{PL}$	Path loss	[dB]
$P_R(i)$	Received optical power from LOS link of i^{th} LED	[W]
$P_R(total)$	Total received optical power	[W]
Py_R, Py_G, Py_B	Parity bits (red, green, and blue, respectively)	
SLA_v	Side-lobe attenuation in vertical direction	[dB]
$S_T(\lambda)$	Transmitter spectral power distribution	[W/nm]
$V(\lambda)$	Luminosity function	
α	Incident angle	[º]
β	Irradiation angle	[º]
$\boldsymbol{\eta}$	Luminous efficacy	[lm/W]
$\theta^{"}, \phi^{"}$	Zenith and azimuth angles, respectively	[º]
θ_{3dB}, ϕ_{3dB}	Vertical and horizontal 3dB beamwidth of an antenna, respectively	[º]
$\boldsymbol{\theta}$	Incident angle	[º]
$\boldsymbol{\lambda}$	Wavelength of the carrier/channel	[m]
$\Phi_{1/2}$	Semi-angle at half illuminance	[º]
Φ_v	Luminous flux	[lm]

$\boldsymbol{\phi}$	Angle of irradiation	[º]
$\boldsymbol{\Omega_{max}}$	Full beam angle	[º]
$\boldsymbol{\Omega_r}$	Receiver solid angle from the transmitter	[º]
$\boldsymbol{\Omega}$	Solid angle	[sr]

1 Introduction

Mobile applications and the growth of data have conducted to a wide use of RF technology for communication and due to this increasing traffic demand, the RF band is becoming scarce. The use of an alternative wireless technology is required. Visible Light Communication is a wireless technology that uses radiation in the visible light spectrum to encode and transmit information [1] - [9].

Traffic lights are the main infrastructure to control the access in road intersections since their appearance. This technology, as well as any other traffic infrastructure, such as, stop signs, is being challenged by the progress of intelligent transport systems, and it is expected to be replaced by more efficient structures in the near future. An intersection manager (IM) may be needed to improve traffic management by sharing information with vehicles [10].

Nowadays, vehicles are equipped with computers and sensors, which provide them with the ability to recognize and interact with their surroundings in an almost autonomous way [11].

Trajectory redesign and real-time traffic planning are two of the challenges considered to improve traffic management. They can be achieved with the introduction of navigation, guidance, and vehicle control methods and with road traffic control expertise and analytical procedures [10].

1.1 Goals of the dissertation

The main goal of this dissertation is the characterization and test of communication links based on VLC technology for road management applications.

To achieve high frequency switching, the light source used is the LED, which can also be used for illumination. The use of RGB trichromatic LED as transmitter and a-SiC:H based photodetector as receiver is proposed.

The share of information between vehicles and with infrastructures is achieved through modes of communication V2V, V2I and I2V.

1.2 Structure of the report

For better understanding of the work developed, this report is divided into the following chapters.

Chapter two is dedicated to the research and study of the subject of this dissertation. The concept of VLC is explained here, as well as the equipment, the architecture, and the application of VLC in connected vehicles. VLC's advantages and challenges, a propagation model and the various types of modulation are also presented.

Chapter three describes the methodology used in this dissertation as well as a few important concepts for better understanding of the work, such as footprint and phasing diagram.

Chapter four is dedicated the simulation tool, where the application developed using the MATLAB software is described. The method and parameters obtained from simulations such as emitted power, pathloss, emitter and channel gain, link budget, calibration step and frame format are described in this chapter.

Chapter five is the results chapter, where results from simulation and laboratory measurements such as coverage map, footprint map, calibration curve, tested scenario, decoding process and the graphical user interface are presented and discussed.

Chapter six summarizes the main conclusions obtained in this dissertation and presents a few guidelines for future work.

1.3 Dissertation output

The work developed was supported by project IPL/IDICA/2020/Geo_Loc/ISEL and, within this research, presented at different Web of Science conferences and published in the respective peer-reviewed proceedings:

- P. Louro, M. Vieira, P. Vieira, J. Rodrigues, M. de Lima, "Geo-localization using indoor visible light communication," Proc. SPIE 11772, Optical Sensors 2021, 117720J (18 April 2021); doi: 10.1117/12.2589477 (conference SPIE Europe 2021, digital forum)
- M. A. Vieira, M. Vieira, P. Louro, M. de Lima, P. Vieira, "Vehicular Visible Light Communication in a Two-Way-Two-Way Traffic Light Controlled Crossroad", SENSORDEVICES 2021, Atenas, 14-19 November 2021.
- P. Louro, M. Vieira, M. A. Vieira, M. de Lima, J. Rodrigues, P. Vieira, "Footprint model in a navigation system based on Visible Light Communication", SENSORDEVICES 2021, Atenas, 14-19 November 2021.
- M. A. Vieira, M. Vieira, P. Louro, M. de Lima, P. Vieira, "Vehicle Visible Light Communication at a Four-Legged Traffic Light Controlled Crossroad", International Journal on Advances in Telecommunications, June 2022.

A best paper award was presented to manuscript “Vehicular VLC in a Two-Way-Two-Way Traffic Light Controlled Crossroad” at the conference SENSORDEVICES 2021 which resulted in the extended version “Vehicle Visible Light Communication at a Four-Legged Traffic Light Controlled Crossroad”.

The MATLAB code produced in this work to model the VLC link is available at the GitHub public repository hosted in the Department of Electronics, Telecommunications and Computers Engineering of ISEL (ISEL-DEETC).

2 State of the Art

The first step to achieve the goal of this dissertation is studying the existing literature, which is the primary purpose of this chapter.

Several concepts acquired during the research about Visible Light Communication (VLC), will be summarized here.

2.1 VLC, Visible Light Communication

Visible Light Communication is a technology for short distance wireless applications. It is an alternative for the Radio Frequency (RF) technology. The mobile applications and the growth of data has driven to a wide use of RF for communication and due to this increasing traffic demand, the RF band is becoming scarce potentially leading to congestion and decrease in the maximum data rate. Thus, the use of an alternative wireless technology is necessary [1] - [9].

VLC uses visible light as the mean of transmitting information and its wavelength varies from around 380 nm to 750 nm, corresponding to the spectrum from 790 THz and 430 THz, respectively. The visible light spectrum is almost completely unexplored for communication purposes, which makes it a great alternative or complement to RF technology. VLC offers larger bandwidth than the RF technology [2] [3] [7] - [13].

VLC works by modulating the intensity of the light and transmitting it by the transmitter at a rate above the perceived by the human eye [7] [13] - [15].

Currently, the use of traditional lamps (incandescent bulbs) is fading due to its low energy efficiency, and it is being replaced by the more efficient LED lamps [2] [8].

2.1.1 Equipment (transmitter and receiver)

The transmitter commonly used in VLC systems is the Light Emitting Diode (LED). White LEDs are often used for illumination in both indoor and outdoor spaces, as the perceived color of objects under this light resembles its colors in natural light [2] [7] [13] - [16].

The white LED can be obtained by combining a blue LED with a yellow phosphor coating or by mixing different colors in a RGB (Red, Green, Blue) LED. The first method is of easier implementation and lower cost but limits the modulation bandwidth available [2] [16] - [18]. The use of RGB LED is proposed in this dissertation.

The RGB LED is advantageous, as it can be operated at a faster rate since it does not have the yellow phosphor layer that causes slow response. Besides, it presents three junctions that if properly modulated provide additional bandwidth [2].

The LED has the potential to be used for both illumination and communication due to its capability of switching to different light intensities at a very fast rate. For this reason, the LED is used in VLC for high-speed data transfer. It presents benefits like longer lifespan, low heat generation, high tolerance to humidity and low power consumption [2] - [8] [13] - [20].

The receivers for this technology are photodiodes and imaging sensors. When exposed to light, the photodetector provides high sensibility, linear response and generates an electrical signal. The ability to respond quickly allows high speed communication. Image sensor is more tolerant to interference caused by light [2] [6] [10] [13].

In VLC, the transmission medium used is free space [8].

2.1.2 Architecture

A proposed architecture for a VLC system is shown in Figure 2.1. On the transmitter side, the data is encoded, modulated, and converted into light that will then be emitted. The receiver extracts the data, converts it in an electrical signal and decodes it to obtain the transmitted information [2] [10].

The first module (transmitter) is responsible for the modulation and conversion of data from digital to analog. The dimming module maintains the desired level of illumination. The driver circuit combines the input data from the transmitter and dimming module, and transmits the result to the LED, to be transmitted [2] [21].

The data is transmitted through the optical channel (space between transmitter and receiver) [21].

The light received by the photodiode is filtered and amplified. The last module (receiver) converts the analog signal to digital and demodulates and decodes this signal [2] [21].

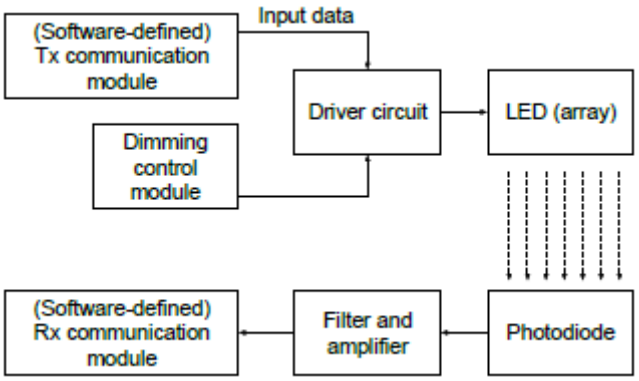

Figure 2.1: A block diagram showing various modulates of VLC transmitter and receiver [2].

Both communication modules (transmitter and receiver) are software defined, where modulation/ demodulation can be programed [2].

2.2 VLC in Connected Vehicles

Traffic congestion is one of the major problems with the increasing number of vehicles and there is a need to make roads safer by preventing and reducing crashes. VLC works with LEDs that have communication and illuminations functions [22].

Traffic infrastructures, such as streetlights and traffic signals, as well as vehicle lighting systems, are being equipped with LEDs, which makes VLC suitable for automotive applications. The information is broadcasted via streetlamps or traffic signaling [10] [13] [21] - [24].

Self-driving and remote driving are two emerging technologies for vehicular communications. The study of vehicle to everything (V2X) communication is required to provide high reliability, low latency, security in the exchange of driving and ambient data. The use of VLC in outdoor scenarios is meeting new opportunities due to the rising popularity of LEDs [10] [25].

Road safety, automotive communication, efficiency of road transportation, traffic light ans public illumination systems are a few examples of the usage of VLC for outdoor scenarios. One of the main goals is controlling the arrival of vehicles and crossing of the intersection at times that minimize delays [10] [12] [25].

Collision avoidance and platooning systems demand cm-level precise vehicle localization, highly reliable and available under harsh road conditions. VLC based vehicle localization methods such as Visible Light Positioning (VLP) might be able to offer this kind of accuracy [26].

The use of VLC for outdoor applications, such as vehicular systems, presents more challenges than in indoor applications: the light interference caused by solar radiation, road lights, building lights and other sources of light and the weather. The majority of VLC vehicular systems mitigate the effects of environment interference by using a filter, MIMO techniques (such as aligning photodiodes to the transmitters) or equipment that are less susceptible to interference (for example, image sensor) [2] [21].

The current infrastructures for traffic management, such as signs and traffic lights, will need to be replaced by other infrastructures that are more effective. In the case of vehicles, headlamps and taillights are equipped with VLC transmitters and receivers. This facilitates communication between vehicles and with infrastructures [10] [21] [23] [27].

2.2.1 Modes of communication

There are three modes of communication for VLC assisted vehicular systems: Vehicle to Vehicle (V2V) communication, where vehicles communicate with other vehicles in their proximity; Vehicle to Infrastructure (V2I) communication, where vehicles communicate with traffic infrastructures; and Infrastructure to Vehicle (I2V), where infrastructures such as traffic lights can transmit information to vehicles [10] [21].

These modes of communication are important to share information in real time. Vehicles share information about their status, traffic information and about surrounding objects at different locations. This cooperation between vehicles or with infrastructures is important to improve the efficiency and safety in traffic [10] [21] [23] [28].

2.3 VLC Advantages

VLC presents many advantages. Some are general and others are particular to the vehicular scenario.

2.3.1 General VLC Advantages

Due to its high frequency, visible light is not able to penetrate most objects or walls and can be confined inside a well-defined zone. This is especially useful when creating small cells with reduced interference. This characteristic makes communication by VLC more secure than by RF [2] [7] [8] [13] [14] [20].

The simple design for functioning, efficiency, and geographical distribution are factors that create a great potential for the use of VLC. The cost of the technology is reduced since the spectrum is not regulated. The technology can also achieve high data rate, even more if associated with MIMO (Multiple Input Multiple Output) [7] [8] [12] - [20].

VLC is very versatile and can be used for communication and illumination. It can also be used for localization, especially in indoor navigation as an alternative to Global Positioning System (GPS). Low power consumption and non-interference with electromagnetic equipment are other advantages of the optical spectrum. Additionally, visible light is not harmful to humans [7] [8] [13] - [20].

2.3.2 Vehicular VLC Advantages

Traditional intersection generates a certain impact on trip delays which is a factor that may lead to waste of natural and human resources [10].

Information regarding a vehicle is available in real time and drivers can adjust their driving conditions, reducing the risk of collisions. Users can also access internet through LEDs installed in street and traffic lights [2] [14].

Vehicular communication systems have various goals, but the most important one is road safety. Dedicated Short-Range Communication (DSRC) is one of the technologies to assist V2V communication [2] [23].

In [2], authors presented a few advantages of VLC when compared to DSRC:

- VLC is less complex due to lower multipath effect and the cost is also lower since LEDs are already being installed in vehicles.
- Vehicles in LOS suffer less interference.
- Visible light is very directive and that provides a sub-meter accuracy for positioning.
- VLC is also very secure since possible attacks could only happen in LOS range, with an easy exposure of the attacker.

2.4 VLC Challenges

To apply VLC in outdoor scenarios, the following challenges must be addressed: robustness to noise, communication range, improving mobility, distance measurement and visible light positioning, improving data rate, etc. [12].

Robustness to noise – in outdoor scenarios, the communication is disturbed by numerous sources of light. An alternative to this problem is to move the communication to a band that differs from the band used by the interfering sources of light. However, when the sun is the source of interference, the use of filters is necessary. As VLC systems are also affected by water (snow, rain, fog) or dust, another way to counteract these effects is by reducing the Field of View (FOV) [12].

Communication range – vehicles interfere on areas greater than the area of communication, which may cause reliability issues. However, for wider distances, accidents are less likely to occur, which means that short distances are crucial to infer on system reliability [12].

Improving mobility – narrowing the FOV is a way of reducing noise and increasing Signal-to-Noise Ratio (SNR), but this reduces mobility. One possible solution for this problem is the use of a tracking mechanism that uses a camera with active control of position. With this solution it is possible to keep the narrow FOV, but the design is complex. Other solutions are proposed such as the use of a light sensor array or the use of multiple photodetectors oriented at different reception angles [12].

Distance measurement and visible light positioning – the vehicle's location and surroundings is very important in safety applications. Modern vehicles use various types of positioning sensors, besides GPS, that are expensive. VLC could be used for to provide a high accuracy positioning, that is cost efficient and less complex [12].

Improving data rate – it is important to improve data rate as long as it does not affect the other concerns previously described. Higher data rate is achieved by implementing more complex modulations. Another way to improve data rate is by introducing MIMO techniques [12].

2.5 Channel Model and Propagation Characteristics

As in any other technology, a method of studying the propagation environment is by analyzing the transmitted and received power, the path loss and the multipath, caused by reflection. When dealing with the visible range it is important to set clear the difference between photometric and radiometric parameters. Photometric parameters are the characteristics of light that are measured as viewed by the human eye. Radiometric parameters determine the characteristics of radiant electromagnetic energy of light [2].

In [2] authors present/propose the following channel model for propagation of visible light.

2.5.1 Luminous Flux

According to [2], luminous flux F_T is the power transmitted by the LED and two ways can be used to calculate it, depending on which parameter is available:

Spectral Integral – uses the Luminosity Function $V(\lambda)$, which represents the sensitivity of the human eye to each wavelength of the visible spectrum, and the Spectral Power Distribution $S_T(\lambda)$, which represents the power of the LED at the wavelengths of the visible spectrum [2].

$$F_T = 683_{[lum/W]} \int_{380\ nm}^{750\ nm} S_T(\lambda) V(\lambda) d\lambda \tag{2.1}$$

It is necessary to ponder the $S_T(\lambda)$ function with the $V(\lambda)$ since the human eye has different responses to each wavelength. The number 683 is a constant that represents the maximum luminous efficiency [2].

Spatial Integral – this method uses the Luminous Intensity $g_t(\theta)$, which is the measure of the brightness of the LED in a certain direction, and the axial intensity I_0 which is the Luminous Intensity at 0º solid angle. Ω_{max} is the beam angle [2].

$$F_T = \int_0^{\Omega_{max}} I_0 g_t(\theta) d\Omega \tag{2.2}$$

2.5.2 Received Flux

The received power/ flux F_R is calculated based on the relative positions of the transmitter and receiver, as seen in Figure 2.2 [2].

$$A_r \cos(\alpha) = D^2 \Omega_r \tag{2.3}$$

$$F_R = I_0 g_t(\beta) \Omega_r \tag{2.4}$$

Where:

A_r – receiver's area

α – angle between the receiver normal and the transmitter-receiver line (incident angle)

D – distance between receiver and transmitter

Ω_r – receiver solid angle observed from the transmitter

β – transmitter viewing angle (irradiation angle)

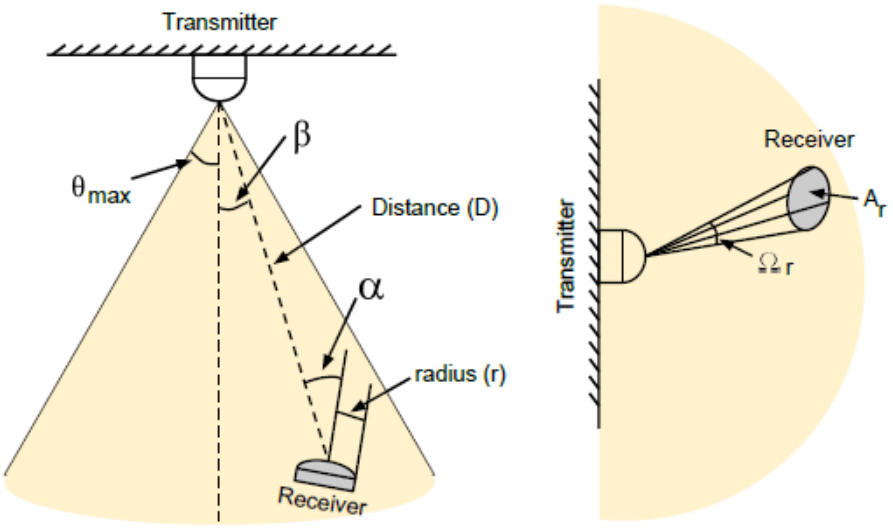

Figure 2.2: Relative position of transmitter and receiver in LOS settings [2].

2.5.3 Path Loss

The path loss L_L, in line-of-sight free space propagation can be presumed to be unrelated to the wavelength [2]. It can be calculated using following equation:

$$L_L = \frac{F_R}{F_T} \tag{2.5}$$

It is considered a Lambertian beam distribution for the LED, which means that the spatial luminous intensity distribution is a cosine function:

$$g_t(\theta) = \cos(\theta)^m \tag{2.6}$$

Where m is the order of the emission, that depends on the semi-angle at half illuminance of the LED, $\Phi_{1/2}$ [2].

$$m = \frac{\ln(2)}{\ln\left(\cos \Phi_{1/2}\right)} \tag{2.7}$$

Combining equations (2.2), (2.3), (2.4) and (2.6) in equation (2.5) the path loss for a Lambertian LED is:

$$L_L = \frac{(m+1)A_r}{2\pi D^2} \cos \alpha \cos(\beta)^m \tag{2.8}$$

2.5.4 Multipath

The multipath $P_R(total)$ can be calculated as the sum of the received power of each LOS link $P_R(i)$, within the receiver's FOV [2].

$$P_R(total) = \sum_{i=0}^{N} P_R(i) \tag{2.9}$$

2.6 Modulation

In VLC, it is not possible to encode data using amplitude or phase modulation. The alternative is to adjust the intensity of the emitted light [2].

As in any communication technology, it is desired to use a modulation prone to ensure high data rate. It is also important to satisfy the following requirements regarding the perceived light by the human eye [2]:

- Dimming: adjusting the level of illuminance according to the activity. It is essential to modulate the data in a way that any level of dimming is supported.
- Flicker mitigation: variation in brightness should not be noticed by the human eye. This variation should occur at a very fast rate to avoid damaging effects.

2.6.1 On-Off Keying (OOK)

OOK is one of the simplest modulations regarding the hardware and works by switching the LED between the on and off states. The off state is not literal, the intensity of the light is lower than the intensity assigned to the on state [2] [18].

This modulation is appropriate for applications that value the communication distance more than the data rate [10].

Dimming can be achieved by attributing different light intensities to the on and off states and without any extra communication overhead. The data rate achievable is the same as the data rate from the implementation of Non-Return-to-Zero (NRZ) OOK. The disadvantage is that at lower dimming levels, the communication range is reduced. By using lower intensities, it is possible for the LED to change the color since it is being operated at a lower current [2].

Another way to achieve dimming is using compensation periods. Instead of changing the intensity of each state, compensation periods will be added creating the on or off periods, depending if the LED is fully turned on or off. If the desired dimming is greater than 50%, on

periods will be added and if it is less than 50%, off periods will be added. The disadvantage of this method is the reduction of data rate, but the communication range stays unaltered since the intensity of on/off periods stays the same [2].

2.6.2 Pulse Modulation Methods

The lower data rate obtained by OOK has motivated the development of modulations based on pulse width and position [2].

In Pulse Width Modulation (PWM) the pulse carries the signal in square waves and its width is adapted according to the required level of dimming. Dimming can occur without alteration in intensity level of the pulse. The limited data rate of this modulation can be improved by combining PWM with DMT (Discrete Multitone) [2].

In Pulse Position Modulation (PPM) the method is based on pulse position instead of width. This means that the symbol is divided in several slots, all with the same duration, and the slots are used to transmit the pulses. Further variations of PPM were implemented to improve the low spectral efficiency and data rate [2].

2.6.3 Orthogonal Frequency Division Multiplexing (OFDM)

This modulation uses a parallel sub-stream to transmit data that result from channel division and high data rate is achievable by transmitting orthogonal sub-carriers [2] [18].

There are two OFDM techniques for converting bipolar signals to unipolar: Asymmetrically Clipped Optical OFDM (ACO-OFDM) and DC-biased Optical OFDM (DCO-OFDM) [2].

In Asymmetrically Clipped Optical OFDM (ACO-OFDM) only odd subcarriers are modulated which makes the time domain signal symmetric [2].

In DC-biased Optical OFDM (DCO-OFDM) all subcarriers are modulated adding a positive direct current to make the signal unipolar [2].

Dimming support in this modulation is limited [2].

2.6.4 Color Shift Keying (CSK)

This modulation was proposed specifically for visible light communication to solve the lower data rate and limited diming support of other modulations. The signal is modulated by regulating the intensity of each LED in an RGB LED, also known as TriLED (TLED) [2].

Table 2.1 compares advantages and disadvantages of each modulation when implemented in VLC technology.

Table 2.1: Advantages and disadvantages of various modulations used in VLC [2] [9] [27].

Modulation technique	Advantage	Disadvantage
OOK	• Simplicity and ease of implementation.	• Low data rate, particularly when dealing with different levels of dimming. • Reduced range or color shift may occur. • Limits spectrum efficiency.
PWM	• Dimming is achieved without changing the intensity of the pulses, therefore no color shift.	• Limited data rate.
PPM	• Simplicity. • Power efficiency.	• Low spectral efficiency. • Low data rate.
OFDM	• Transmits multiple bits per channel. • Deals with inter-symbol interference and multipath fading.	• Challenges in implementation.
CSK	• Overcomes lower data rate. • Dimming support. • Flickering is not a problem.	

3 Proposed Test Scenario (Methodology)

By using VLC connected cooperative drive, it is expected an increase of security and throughput of traffic intersection. The road spaces and structures have developed to fit the needs of road traffic control [10].

A redesign of intersection trajectories is proposed. This is achieved by applying several methods and knowledges about navigation and road traffic control of vehicle [10].

An intersection is determined by their physical and functional areas. The functional area includes two elements: lane changing/ request distance and responding message or queue storage distance [10].

The proposed scenario is represented in Figure 3.1:

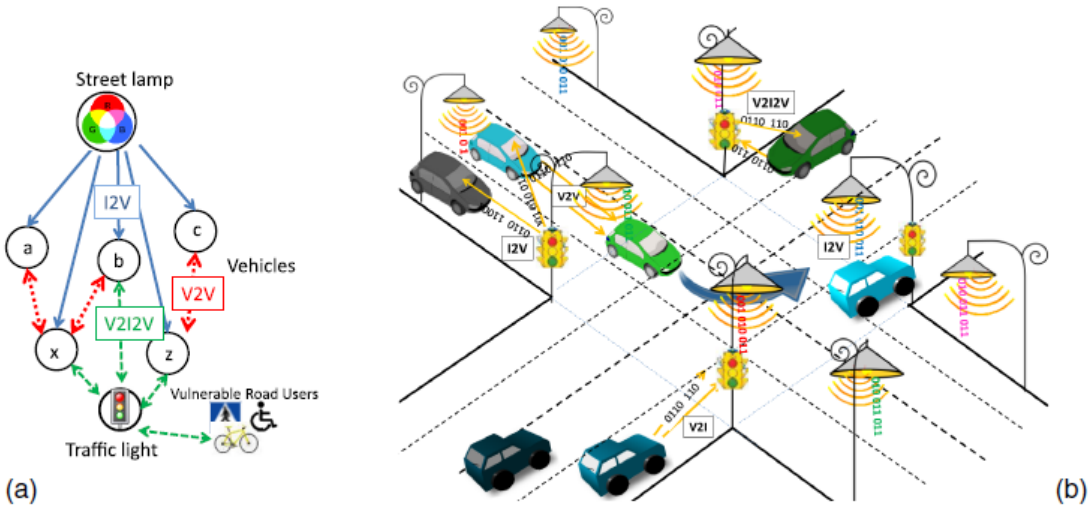

Figure 3.1: Illustration of the proposed I2V2V2I2V communication scenario: (a) generic model for cooperative vehicular communication. (b) Connected vehicle communication link [10].

The transmitter sends a message that is processed by the receiver located on the rooftop of the vehicle. The information can then be resent to another vehicle using the headlight (V2V) or a “request” to change route, depending on the occupied lane, is sent to a crossroad receiver (V2I). The local controller emitter sends a “response” message to the vehicle (I2V), establishing bidirectional communication (V2I2V) [10].

White light tetrachromatic sources are utilized to provide illumination and communication, and a different channel is provided for each chip. Only one chip is modulated to transmit data, while the other three are used to supply current for white light perception. Therefore, each transmitter ($X_{i,j}$) is assigned a color X (R, G, B or V) and the horizontal and vertical ID position (i, j) in the network [10].

In Figure 3.2 it is shown the considered plan and generated joint footprint. In this plan, four traffic flows are considered: one from west (W) with vehicles “a”, “c” and “d”, a second flow from east (E) with vehicle “b”, a third flow from south (S) with vehicle “e” and finally the last flow, from north (N) with vehicle “f”. Each vehicle has its own intention, whether that is keeping straight forward or turning to another direction (right or left) [10].

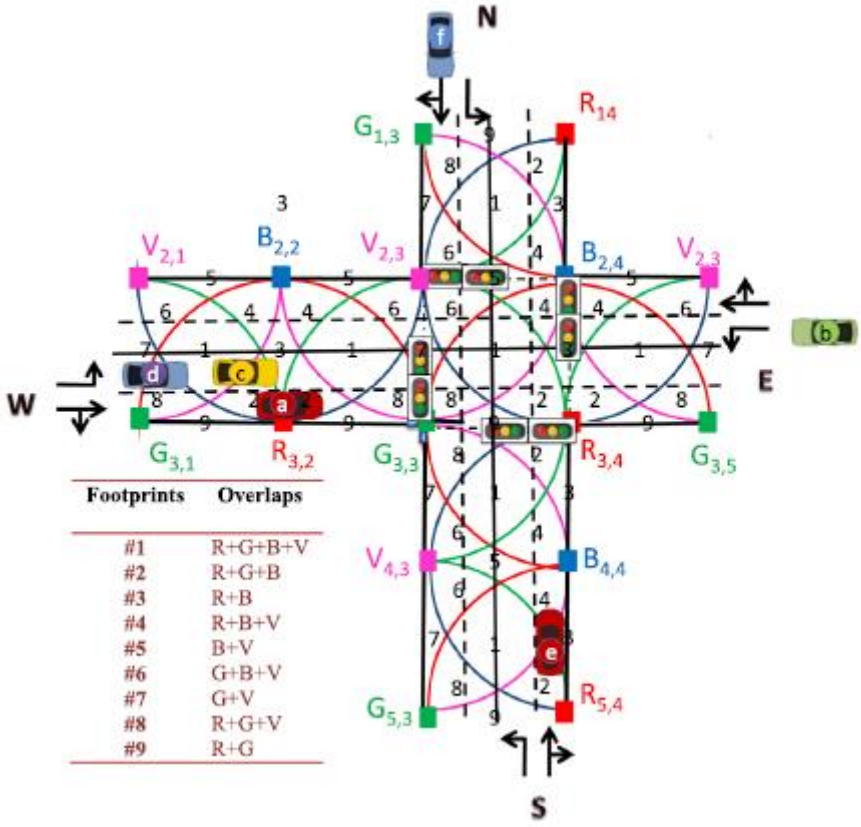

Footprints	Overlaps
#1	R+G+B+V
#2	R+G+B
#3	R+B
#4	R+B+V
#5	B+V
#6	G+B+V
#7	G+V
#8	R+G+V
#9	R+G

Figure 3.2: Lighting plan and generated joint footprints in a crossroad (LED array = RGBV color spots) [10].

To receive information, the receiver should be placed at the transmission range of the transmitter. The transmission range circle may overlap, as seen in Figure 3.2, and there are nine possibilities, called footprints. The distinction of the footprints is important for the localization of the vehicle in the cell and for encoding/decoding the information [10].

The cell is the element resulting of the intersection of the many lines of the grid. They are identified by the LED at the top left corner. The grid size was chosen to fit the footprint, avoiding an overlap in the receiver from the data from adjacent grid points. This means that each cell receives data from one LED/channel of each color [11].

It is necessary to distinguish the head/leader vehicle, which is the first vehicle on a lane or the second if the first has begun crossing the intersection region [10].

To build a V2V system, a follower and the leader share messages between them that can be resent to the next vehicle or near infrastructure [10].

When approaching the intersection, the driver has already chosen the lane, according to their destination. The vehicle sends a “request” message to the receiver interconnected to the intersection manager (IM). The intersection manager then acknowledges the message and sends a “confirmed vehicle” message (as long as it does not constitute a risk of conflict with any other vehicle). Once the “confirmed vehicle” message is received, the vehicle is required to follow along specific footprint regions given by the intersection manager [10].

3.1 Experimental results

The modulation used was OOK and it was considered a 32-bit codification. The frame used to transmit data is divided into three blocks, if the transmitter is a streetlamp or a headlamp (Figure 3.3 (a)), or into four blocks, if the transmitter is the traffic light (Figure 3.3 (b)) [10].

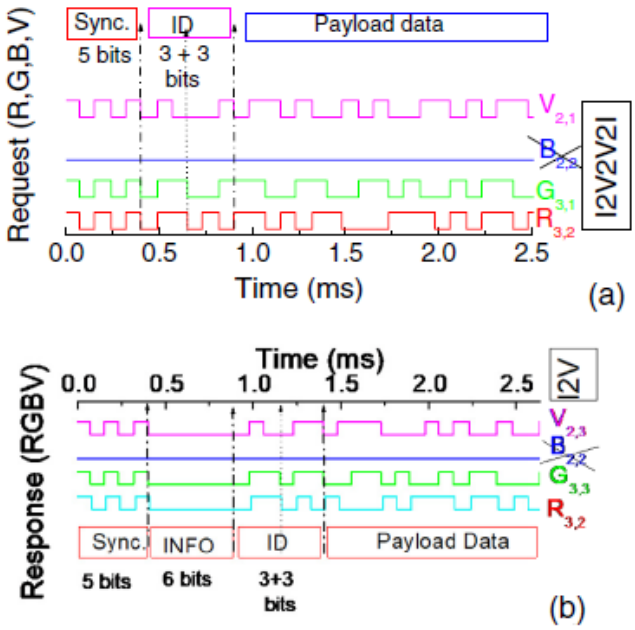

Figure 3.3: Frame structure representation. (a) Codification used to drive the headlights of a vehicle in a request message from footprint #8. R3;2, G3;1, and V2;1 are the transmitted node packets, in a time slot. (b) Encoded message response of the controller to a vehicle located in the crossroad (#1, R3;4, G3;3, B2;4, and V2;3) [10].

The first block is the synchronization block (10101), the last is the payload data and it is also used a stop bit at the end of the frame. The ID block is the ID of the emitter where the first three bits are the code of the line and the last three are the code of the column. In Figure 3.3

(b), the INFO block (000000) is used to indicate that the response is being sent by the control manager [10].

In Figure 3.4 it is displayed a multiplex (MUX) data (signal) due to the transmission of four optical signals in a frame (using the R, G, B and V emitters). The signal can be decoded by attributing each of the 16 possible combinations to a 4-digit binary code [X_R, X_G, X_B, X_V], where the digit is 1 when the respective channel is on and 0 when the channel is off [10].

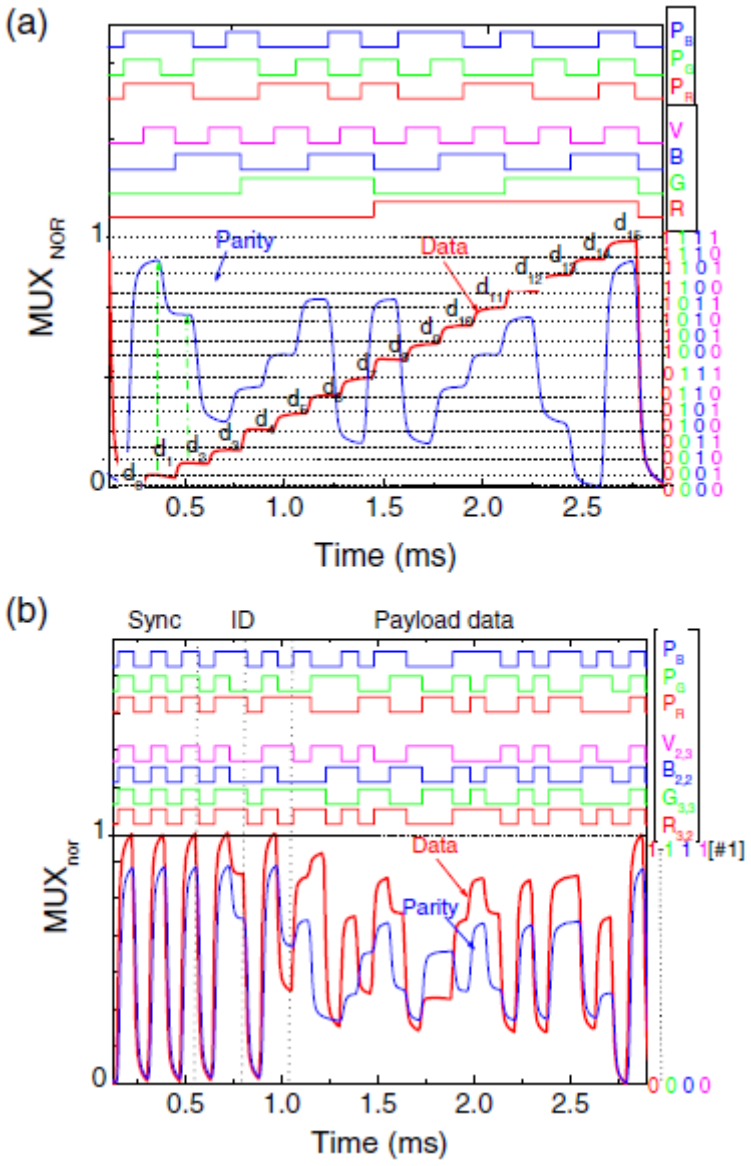

Figure 3.4: Normalized MUX data signals. The parity MUX signal is also superimposed to exemplify the bit error detection. On the top, the transmitted channels packets [R, G, B, V] and parity bits [PR, PG, PB] are depicted. (a) Calibrated cell. (b) Signals acquired by a receiver in positions #1, cell [$R_{3,2}$, $G_{3,3}$, $B_{2,2}$, $V_{2,3}$] [10].

The parity is a mechanism used for checking and correcting the incoming bit errors in the decoding process due to the magnitude proximity of consecutive levels. The parity bits are generated as a function of the transmitted bits, and are defined as [10]:

$$Py_R = V \oplus R \oplus B \tag{3.1}$$

$$Py_G = V \oplus R \oplus G \tag{3.2}$$

$$Py_B = V \oplus G \oplus B \tag{3.3}$$

The parity is encoded and sent with the data, the receiver calculates the parity from the incoming/decoded bits and compares it with the parity to check for errors [10].

A four-input channel transmission requires three parity channels to generate channel redundancy. The encoder generates three parity bits from four input data bits that corresponds to eight (2^3) different levels (Figure 3.4 (a)). By comparing data and parity signal, the transmitted information is retrieved [10].

In Figure 3.5, the normalized MUX signal received by a receiver located in the footprint positions #1, #2, #4, #6 and #8, for an I2V communication, confirms the decoding process [10].

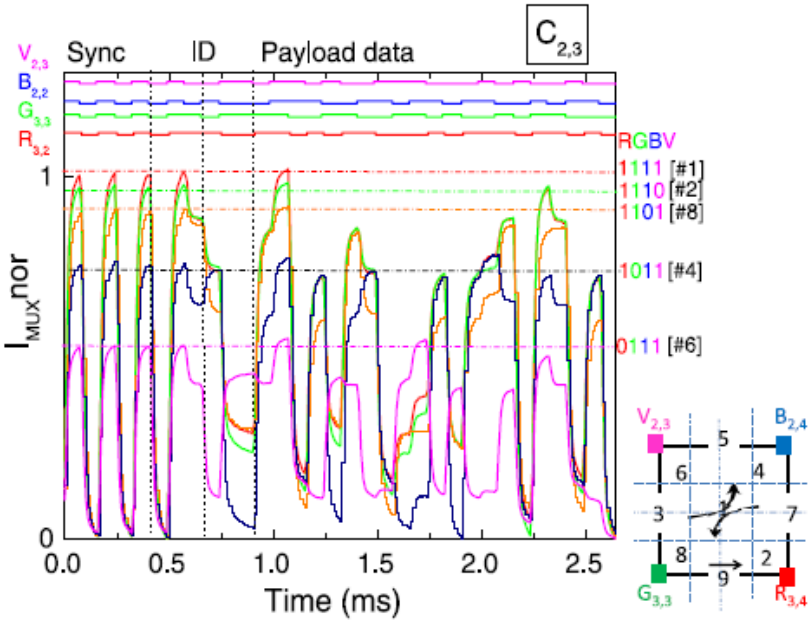

Figure 3.5: Normalized MUX signals acquired by a receiver at the crossroad in positions #1, #2, #4, #6, or #8. On the top, the transmitted channels packets [R, G, B, V] are decoded [10].

After decoding the signals and considering the frame structure it is possible to reveal the position of the receiver and its ID. The footprint is also obtained from the maximum amplitude detected in the synchronization block [10].

3.2 Phasing Diagram

The phasing diagram is an example of the order which the vehicles should follow to safely cross the intersection. One possibility is shown in Figure 3.6. This is especially useful since two maneuvers can occur at the same time without conflict [11].

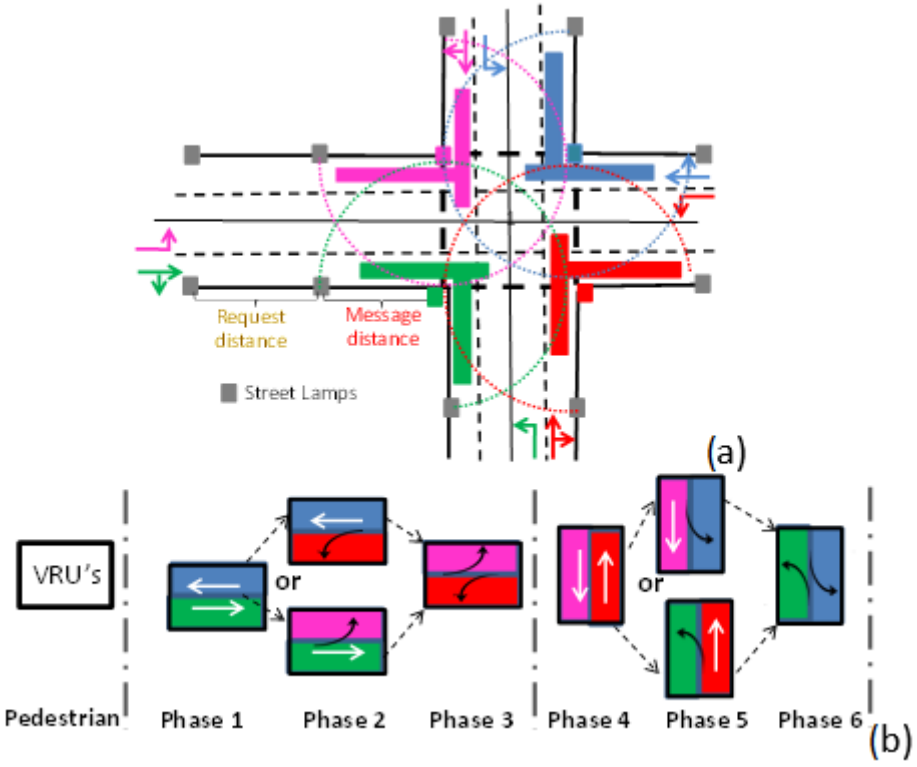

Figure 3.6: (a) Physical area, color poses and channelization. (b) Representation of a phasing diagram [11].

The functional area at the approximation of the intersection consists of two elements: request distance and response/message distance. The vehicles must occupy the right lane if its intention is to keep straight or turn right and it must occupy the left lane if the intention is to turn left. Lane change must be accomplished in the request distance (Figure 3.6 (a)) [10].

West straight/right and South left maneuvers are represented as “green pose”, South straight/right and East left maneuvers correspond to “red pose”, East straight/right and North

left maneuvers are the “blue pose” and finally the “violet pose” are North straight/right and West left maneuvers [11].

4 Description of the Simulation Model

This chapter is dedicated to the description of the model used to characterize the VLC transmitted signals and the VLC signal acquired by the receiver.

The model was implemented in MATLAB and works by reading a BMP file of the road with each LED in its respective position. The emitted power, the wavelength of the LED/channel and the receiver/channel gain are the inputs needed.

The pathloss and the emitter's gain are calculated within the program, which then calculates the link budget and provides outputs, such as, the coverage map, footprint map and the calibration step. The message is encoded following a frame structure, transmitted, and decoded in the receiver.

The steps involved in the development of this model are explained in the following subchapters.

4.1 Emitted Power

The luminous intensity, $I_{N,}$ is the brightness of the LED [2] [17] and it is given in millicandela (mcd) by the datasheet [29]. This value was converted to power P, using the following equations (θ is the aperture angle of the LED):

$$\Omega_{[sr]} = 2\pi(1 - \cos(\theta/2)) \tag{4.1}$$

$$\Phi_{v_{[lm]}} = I_{N_{[mcd]}} \times \Omega_{[sr]}/1000 \tag{4.2}$$

$$P_{[W]} = \Phi_{v_{[lm]}}/\eta_{[lm/W]} \tag{4.3}$$

Where: Ω is the solid angle, Φ_v is the luminous flux and η is the luminous efficacy.

Initially, the intensity used in simulations was taken from the LED's datasheet [29]. Furthermore, it was adapted so that the calibration step (used in encoding/decoding) is closer to the one obtained in the laboratory.

4.2 Path Loss

The path loss PL was obtained from the following equation (4.4) [30]:

$$PL_{[dB]} = 22 + 20\log\frac{d}{\lambda} \tag{4.4}$$

Where: d is the distance between transmitter and receiver, and λ is the wavelength of the channel.

As mentioned before, external factors such as adverse atmospheric conditions affect VLC systems, and they need to be considered (L_{Atm}). Obstacles are another factor to be considered since light cannot penetrate solid object (L_{Obst}).

Considering all these additional factors, the total attenuation L is determined by equation (4.5):

$$L_{[dB]} = PL_{[dB]} + L_{Atm_{[dB]}} + L_{Obst_{[dB]}} \tag{4.5}$$

4.3 Gain

The emitter gain was initially calculated using the 3GPP antenna model [31] used in RF technology and later the same evaluations were adapted to the optical domain using the Lambertian model. The receiver/channel gain was obtained in the laboratory, with the use of a LED as background steady state light that acts as an optical bias to amplify (or attenuate) the signal.

4.3.1 Antenna model

The 3GPP antenna model [31] used as the first approximation to characterize the transmitter is described by:

$$A_{dB}^{"}(\theta^{"}, \phi^{"} = 0°) = -min\left\{12\left(\frac{\theta^{"} - 90°}{\theta_{3dB}}\right), SLA_v\right\} \tag{4.6}$$

$$\theta_{3dB} = 60°, SLA_v = 30\ dB, \theta^{"} = [0°, 180°] \tag{4.7}$$

$$A_{dB}^{"}(\theta^{"} = 90°, \phi^{"}) = -min\left\{12\left(\frac{\phi^{"}}{\phi_{3dB}}\right), A_{max}\right\} \tag{4.8}$$

$$\phi_{3dB} = 60°, A_{max} = 30\ dB, \phi^{"} = [-180°, 180°] \tag{4.9}$$

$$A_{dB}^{"}(\theta^{"}, \phi^{"}) = -min\left\{-\left(A_{dB}^{"}(\theta^{"}, \phi^{"} = 0°) + A_{dB}^{"}(\theta^{"} = 90°, \phi^{"})\right), A_{max}\right\} \tag{4.10}$$

Where:

$A_{dB}^{"}$ – antenna radiation power pattern

$\theta^{"}$, $\phi^{"}$ – zenith and azimuth angles, respectively

θ_{3dB}, ϕ_{3dB} – vertical and horizontal 3 dB beamwidth of an antenna, respectively

SLA_v – side-lobe attenuation in vertical direction

A_{max} – maximum attenuation

Although the antenna model is a good approximation, it is not the most adequate considering the light source that is used. It was further replaced by the Lambertian model.

4.3.2 Lambertian model

As previously stated, the antenna model was replaced by the Lambertian model, which better describes the light distribution from the LED light source [32].

$$m = -\frac{\ln(2)}{\ln\left(\cos\left(\phi_{1/2}\right)\right)} \tag{4.11}$$

$$G = \frac{(m+1)A}{2\pi D_{t-r}^2} I_N \cos^m(\phi)\cos\theta \tag{4.12}$$

Where:

m – order derived from a Lambertian pattern

$\phi_{1/2}$ – half intensity angle

G – channel gain

A – area of the photodetector

D_{t-r} – distance between the transmitter and the receiver

I_N – maximum luminous intensity in the axial direction

ϕ – angle of irradiation

θ – incident angle

4.4 Link Budget

The link budget was calculated from the Friis Transmission Equation (4.13). This is used to obtain the coverage map of the received power.

$$P_{R_{[dBm]}} = P_{E_{[dBm]}} + G_{E_{[dB]}} + G_{R_{[dB]}} - L_{[dB]} \quad (4.13)$$

Where:

P_R – received power

P_E – emitted power

G_E – emitter gain

G_R – receiver gain

L – pathloss

4.5 Calibration Curve

The calibration curve is used in the encoding and decoding processes. Since there are four LED/channels and each one transmits either a 0 or a 1, there are 16 possible combinations (2^4 = 16). During the calibration process, a value was assigned to each of the combination, allowing them to be distinguished and therefore identified as input optical channels.

4.6 Frame Format

The information shared between the transmitter and receiver is transmitted using a pre-defined frame structure. This specification is important so both sides can understand and decode the information that is being provided.

The frame used has 64 bits, plus 5 for synchronization (sync) purposes and 1 to end the frame (end of frame, EOF). It is divided as indicated in Table 4.1.

Table 4.1: Frame structure.

Sync	ID_X	ID_Y	Angle δ	IM	Payload	EOF
5 bits	4 bits	4 bits	4 bits	2 bits	50 bits	1 bit

64 bits

The sync is a fixed pattern of [10101] in all four LED/channels. It represents the beginning of the frame. The ID is obtained from the location of the vehicle. The angle is the orientation of the vehicle, obtained by measuring the angle between the vehicle and the horizontal line, and it is the same for all four channels. The possibilities of pose orientation are shown in Figure 4.1.

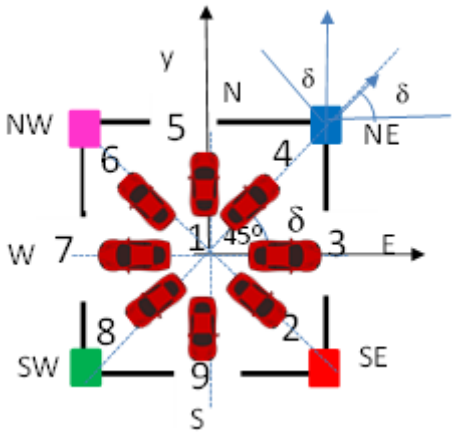

Figure 4.1: Pose orientation [33].

When transmitted in the frame, the angle is attributed values ranging from 2 to 9 that correspond to 315º, 0º, 45º, 90º, 135º, 180º, 225º and 270º, respectively. Number one is the center of the figure and is not considered a valid angle value.

The IM is [00] when the communication is from the vehicle to the IM (request) and [11] when the communication is from the IM to the vehicle (response). It is also the same for all four channels. The payload stores all additional information that might be necessary. Finally, the EOF represents the end of the frame and is a fixed [0] in all four channels.

5 Results and Discussion

Several results of the developed simulations using MATLAB are presented in this chapter.

To simplify the process, the code was developed to simulate only one cell at first. Then, the complexity of the code was increased to include the simulation of more than one cell, until achieving the simulation of four cells. Finally, the proposed scenarios were tested using an intersection with five cells.

5.1 Coverage map

The coverage map allows us to analyze the power distribution in each map. The link budget is evaluated for each point of the map (equation (4.13)) and the results are grouped by color according to a certain range.

The result for one cell is represented in Figure 5.1. The inputs used are described in Table 5.1 and all the values were converted to decibel.

Table 5.1: Link budget input.

Variable	**Value**			
	Red LED	**Green LED**	**Blue LED**	**Violet LED**
$I_{N_{[mcd]}}$	730	650	800	900
$G_{E_{[dB]}}$	Eq. (4.12)			
G_R	5	4	1,7	0,8
$L_{[dB]}$	Eq. (4.5)			

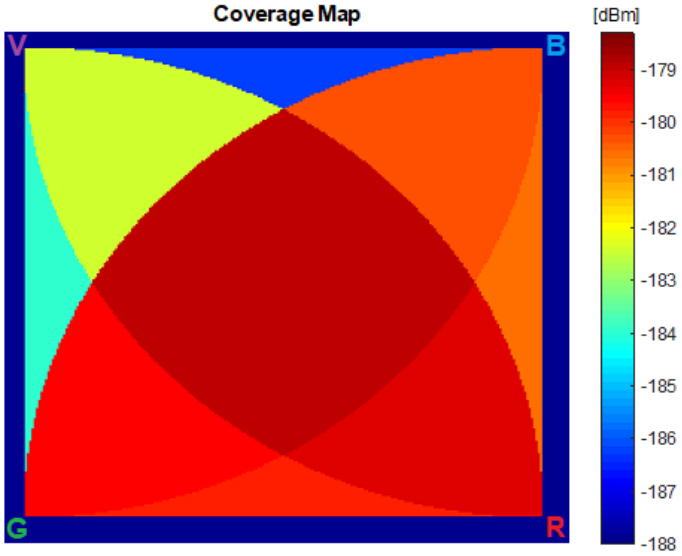

Figure 5.1: Coverage map of one cell.

The cell radius used is 2 cm to match the radius used in the laboratory prototype.

As observed in Figure 5.1, the center of the cell is the location where the received power is higher. Usually, due to pathloss, wider distances correspond to lower power. That is not observed in this case because of the short radius of the cell. The pathloss does not affect much for short distances. It is also observed that the power of the coverage map ranges from -188 dBm to -179 dBm.

5.2 Footprint Map

As explained is chapter 3, the footprints correspond to the overlap of the transmission range circle. Figure 5.2 shows the footprint map of the power distribution derived from the coverage map (Figure 5.1), represented as nine sub-power ranges.

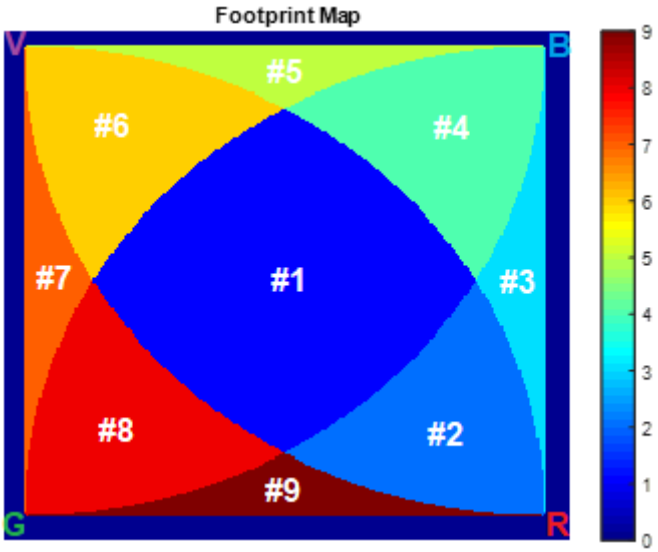

Figure 5.2: Footprint map of one cell.

The transmission range of all four LED/channels overlap in the center of the cell (footprint #1). Adjacent to the center, with a “triangular” shape, there is an overlap of the transmission range of three LED/channels (footprints #2, #4, #6 and #8). On top, bottom, and sides of the cell there are only two LED/channels overlaping (footprints #3, #5, #7 and #9).

5.3 Calibration curve

The calibration curve is used to support the encoding and decoding techniques. Figure 5.3 shows the normalized calibration curve where (a) is the simulated curve and (b) was obtained from measurements in the laboratory.

To obtain the curve, a binary sequency from 0 to 15 is encoded and sent, and by observation of the result the intensity of each LED is adjusted to obtain the best curve possible (the red LED/channel is the most significant bit, and the violet LED/channel is the least significant bit).

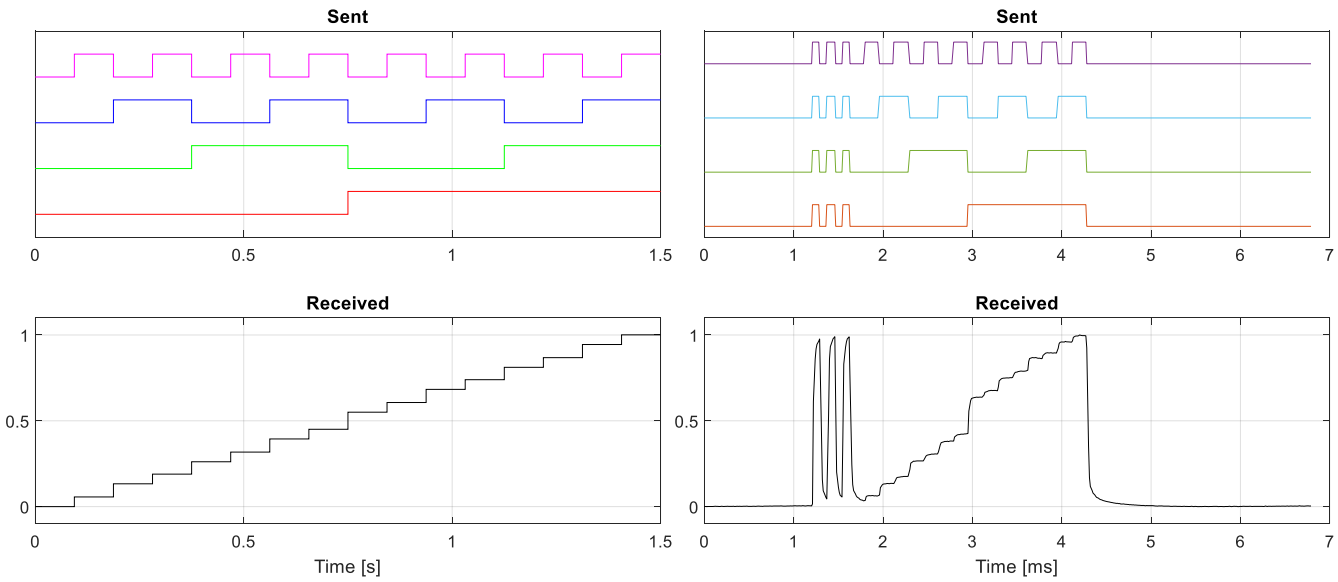

Figure 5.3: Normalized calibration curve. (a) Simulated. (b) Obtained via lab measurements.

As observed in Figure 5.3, the simulated curve and the lab curve are similar.

The red LED/channel introduces more weight to the calibration curve and the signal amplitude is always over 0.5, which is partially due to higher amplification gain of the red light.

The sync pattern is seen in the beginning of the frame in the experimental data (Figure 5.3 (b)).

The simulated curve (Figure 5.3 (a)) presents more uniform steps than the ones obtained by laboratory measurements. These slight differences can be explained due to capacitive effects of the LED that appear in the experimental curve and are not considered in the simulation. This effect may introduce noise in the experimental data which is prone to generate errors in decoding.

5.4 Tested Scenarios

The tested scenario composed of a crossroad with five cells is displayed in Figure 5.4.

The top cell is the cell $B_{1,2}$ but will be referred as cell one, C1 for short. The middle cells are, from the left to the right, $G_{2,1}$, $R_{2,2}$, $G_{2,3}$, or C2, C3 and C4. The bottom cell is cell $B_{3,2}$ or C5 for short.

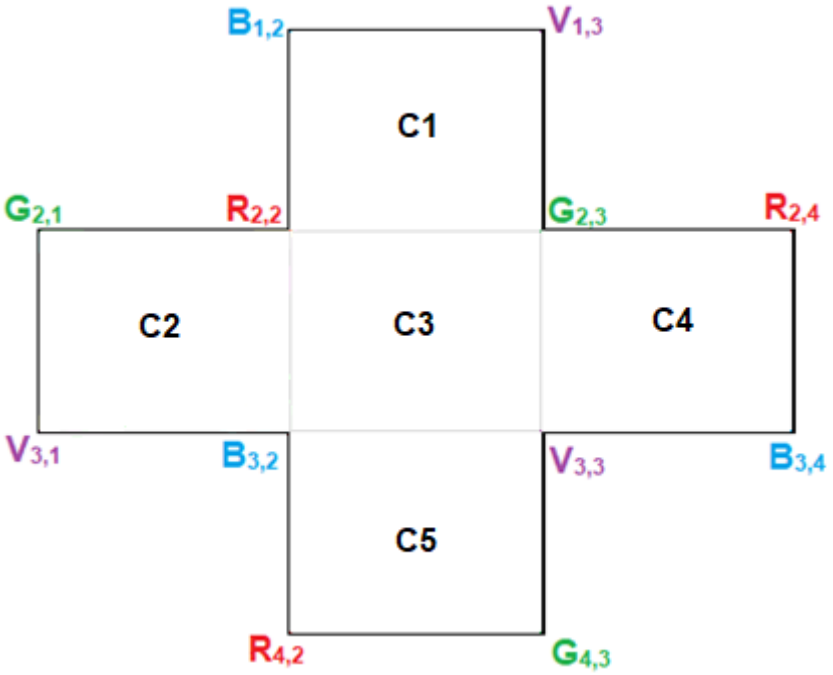

Figure 5.4: Proposed scenario.

It was simulated.in these cells the trajectories of vehicles "a" and "c", illustrated in Figure 5.5. These trajectories show vehicle "a" traveling from West to East along the lane, passing through cells C2, C3 and C4, while vehicle "c" performs a turn left movement, passing through cells C2, C3, and C1. This last trajectory corresponds to a movement from West to North direction.

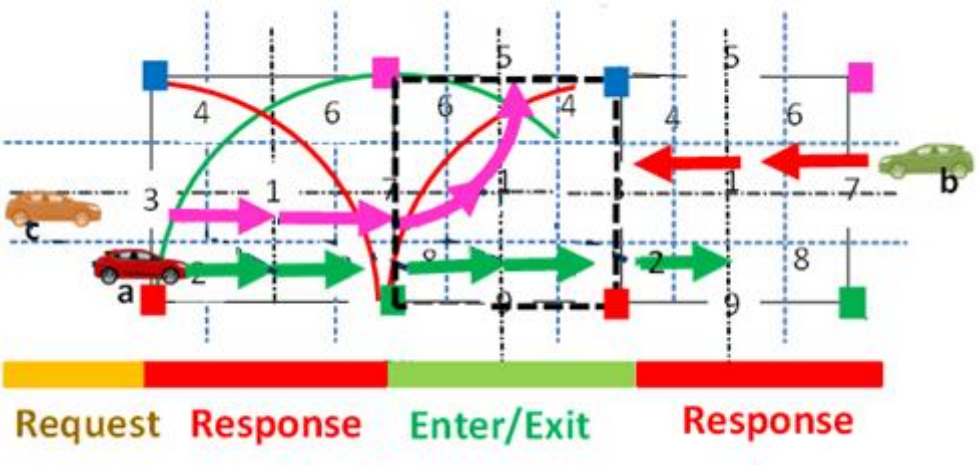

Figure 5.5: Example of vehicle trajectories [11].

In Figure 5.5 the request distance shows where the vehicle sends a request to cross the intersection and the response distance shows where the vehicle receives the response

(permission or rejection to cross) from the IM. The enter/exit distance corresponds to the crossroad.

The experimental result is obtained by encoding a message following the frame structure (Table 4.1) using a program in the laboratory. The message is transmitted via RBG LED [28]. Dedicated receivers based on a-SiC:H/a-Si:H photodiodes with selective spectral sensitivity [34] [35] are used to record the transmitted multiplexed signal.

For testing purposes, it was assumed that all vehicles have received permission to cross and only the cells that correspond to response distance and enter/exit will be demonstrated.

5.4.1 West to East (straight path)

A scenario where the vehicle moves from West to East was the first to be simulated. As shown in Figure 5.6, the vehicle starts in cell C2, before the crossroad, then goes to cell C3 where it occupies three different positions/footprints and ends in cell C4, after leaving the crossroad.

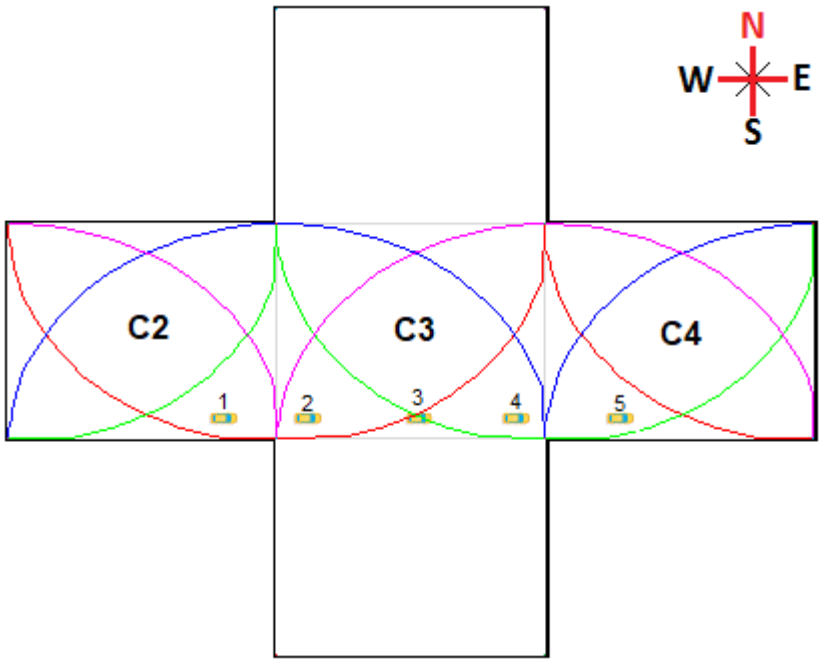

Figure 5.6: Proposed scenario, vehicle moving from West to East.

The following image (Figure 5.7) shows the result of the tests performed in the cell C2.

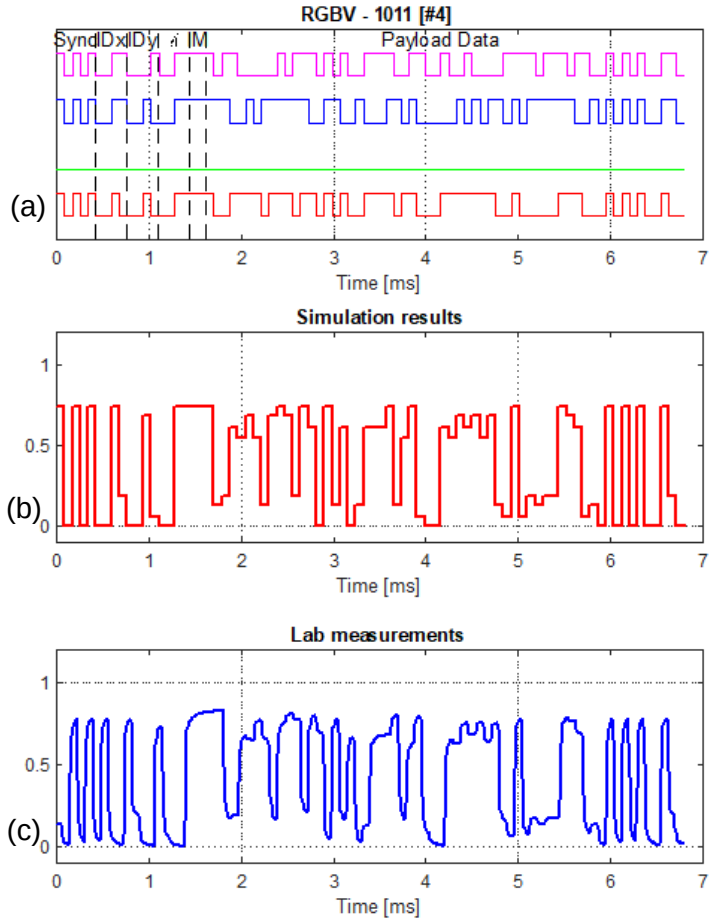

Figure 5.7: Results of the proposed scenario, West to East, cell C2 (position 1), footprint #4: (a) transmitted signals by each channel, (b) simulation of the normalized received signal and (c) normalized experimental received signal.

Under these test conditions the vehicle occupies footprint #4 in cell C2 and receives inputs from channels red, blue and violet. The signals transmitted by each channel are displayed Figure 5.7 (a).

The middle (Figure 5.7 (b)) and bottom (Figure 5.7 (c)) frames are the simulated and measured received signals, respectively. At the receiving end it is possible to observe that the maximum amplitude of the received signal is lower than one (1) due to the absence of the green LED/channel and over 0.5 due to the presence of red LED/channel.

Comparing the received signals (Figure 5.7 (b) and Figure 5.7 (c)) it is possible to conclude that both the simulated and the measured signals are similar. This good agreement shows that the simulation tool is able to reproduce the results from the laboratory, which supports the models used to describe and characterize this VLC link.

There are, however, slight differences especially when it comes to the blue and violet LED/channels. These two are the less intense signals and the differences in the received signal in the presence or absence of either of these LED/channels are less noticeable in the measured signal than in the simulated one. It is also important to point out the capacitive effect of the LED, which means that the flow of charges across its internal junction takes time and sudden changes in the transmitted bits are less perceived.

The frame follows the structure presented in Table 4.1. At the beginning the sync pattern is transmitted, followed by the ID of the cell, the angle, the IM and the payload. The ID is $R_{2,2}$, $G_{UNKNOWN}$, $B_{3,2}$, $V_{3,1}$ (since the vehicle is out of reach of the green LED/channel, it is not known the ID for this particular LED/channel). The angle is 3 ([0011] in binary) which corresponds to zero degrees (0^{o}) and the IM pattern is [11] meaning that this message was transmitted from the IM to the vehicle.

A right turn follows the same protocols. For this specific cell, everything would be the same.

Next, staying in the straight path, the vehicle goes to cell C3, entering the crossroad. The results are displayed in Figure 5.8.

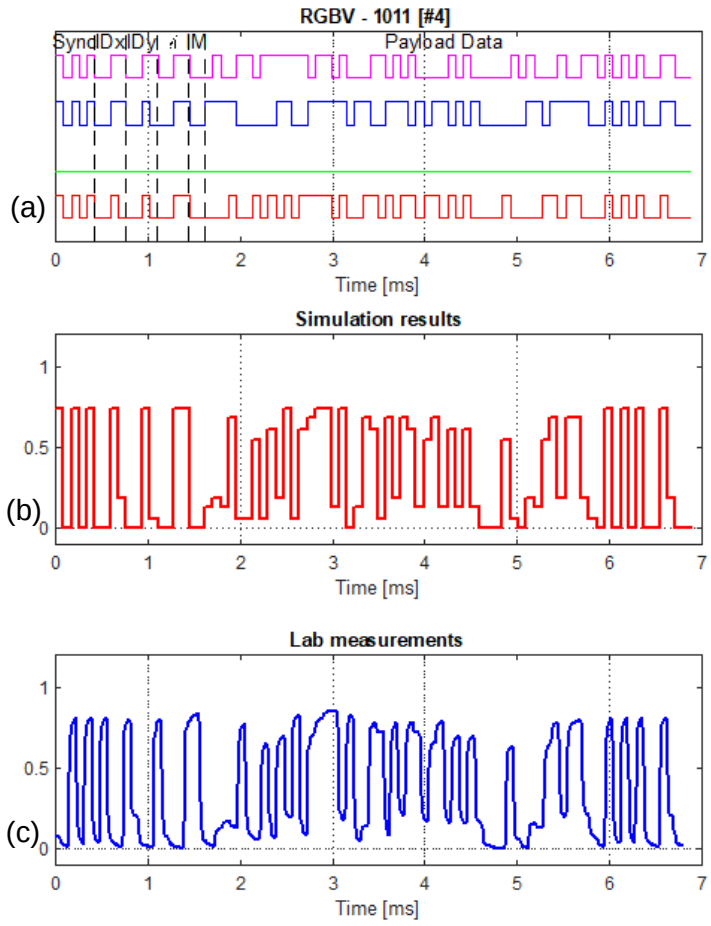

Figure 5.8: Results of the proposed scenario, West to East, cell C3 (position 2), footprint #4: (a) transmitted signals by each channel, (b) simulation of the normalized received signal and (c) normalized experimental received signal.

Just as in Figure 5.7, the signal transmitted by each LED/channel is displayed on the top frame, Figure 5.8 (a). In cell C3, the vehicle at position 2 occupies footprint #4, receiving signals from the red, blue, and violet channels.

At the receiving end (middle and bottom frames, Figure 5.8 (b) and (c), respectively) it is possible to observe that the maximum amplitude of the received signal is once again lower than one (1) due to the absence of the green LED/channel and over 0.5 due to the presence of red LED/channel.

The evidence for reproducibility of the simulation tool can be seen again in Figure 5.8, where the received signals for the simulated and measured signals are similar.

As in cell C2, there are slight differences between the simulated and measured signals. As mentioned before, the presence or absence of the blue or violet LED/channel is less noticeable in the measured signal than in the simulated one.

This frame, as well as all the others, follows the structure presented in Table 4.1. At the beginning the sync pattern is transmitted followed by the ID of the cell ($R_{2,2}$, $G_{UNKNOWN}$, $B_{3,2}$, $V_{3,3}$), the angle (still 3 that corresponds to 0º, since the vehicle is not changing its direction), the IM ([00] meaning that this message is sent by the vehicle to the IM) and the payload.

When turning right in this cell, the angle code would be 2 (315º) and the vehicle would turn to cell C5 instead of going forward to cell C4.

Still, in cell C3 the vehicle moves forward and goes to the next position/footprint, losing the red LED/channel. The correspondent results are presented in Figure 5.9.

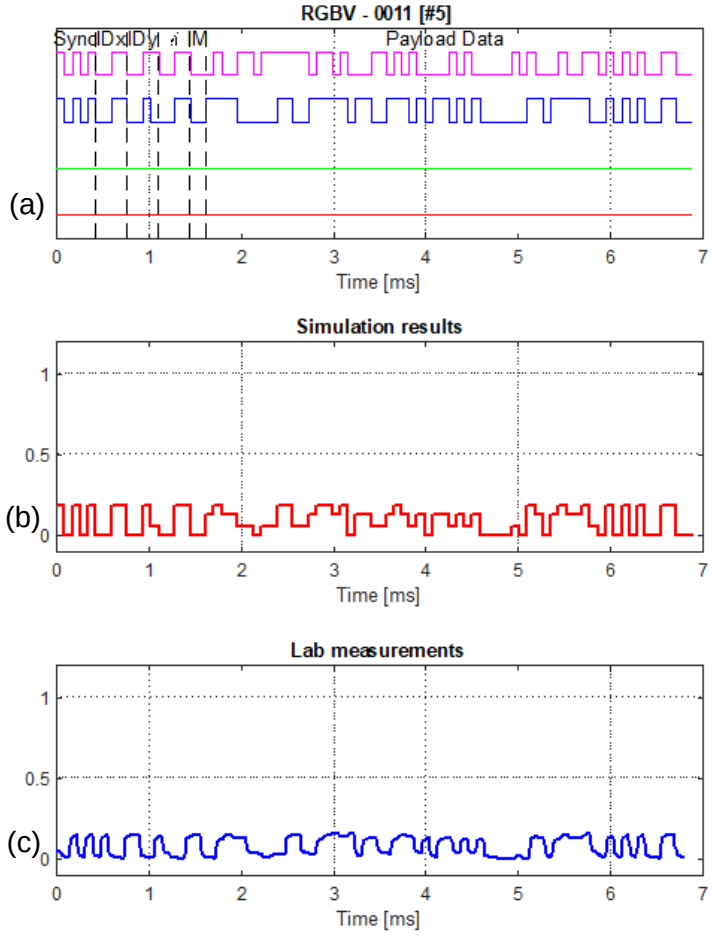

Figure 5.9: Results of the proposed scenario, West to East, cell C3 (position 3), footprint #5: (a) transmitted signals by each channel, (b) simulation of the normalized received signal and (c) normalized experimental received signal.

The vehicle at position 3 of cell C3 occupies footprint #5.

In Figure 5.9 its observed that the maximum amplitude of the received signal is lower than 0.5 due to the absence of red LED/channel.

Once again, it is seen that the simulations were able to reproduce the experimental measurements.

In this scenario, the capacitive effect of the LED makes it more challenging to distinguish the levels of the measured signals, since the only LED/channels present are the low intensity blue and violet LED/channels.

Despite the differences, the frame still follows the structure of Table 4.1. The sync pattern marks the beginning of the frame followed by the ID $R_{UNKNOWN}$, $G_{UNKNOWN}$, $B_{3,2}$, $V_{3,3}$. The angle is still 3 or 0º and IM is still [00].

Finally, the vehicle moves to the final position/footprint in cell C3 (position 4), where the red channel is still absent, but the green LED/channel is present again. The results are shown in Figure 5.10.

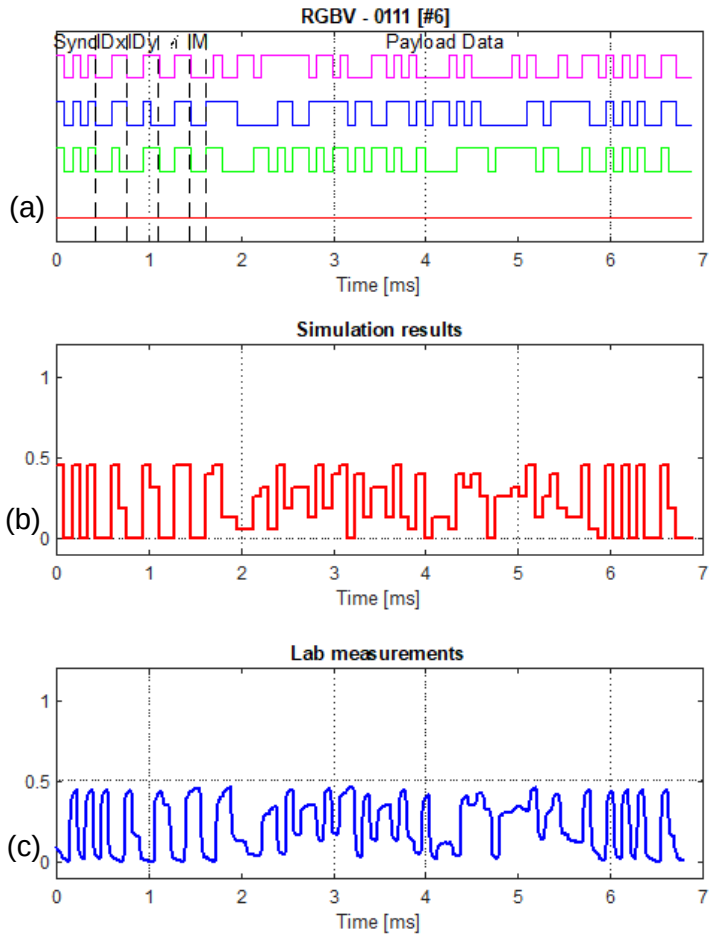

Figure 5.10: Results of the proposed scenario, West to East, cell C3 (position 4), footprint #6: (a) transmitted signals by each channel, (b) simulation of the normalized received signal and (c) normalized experimental received signal.

The vehicle at position 4 of cell C3, occupies the footprint #6 (Figure 5.10).

The results for this position are very similar to the results presented previously. The maximum amplitude of the received signal is lower than 0.5 due to the absence of red LED/channel.

The simulation was able to reproduce the measured signal. The slight differences are also due to the capacitive effects of the LED.

As for the frame, the sync pattern is transmitted at the beginning, followed by the ID $R_{UNKNOWN}$, $G_{2,3}$, $B_{3,2}$, $V_{3,3}$, by the angle (3 or 0º), by the IM ([00]) and by the payload.

In Figure 5.11 it is displayed the results obtained when the vehicle leaves the intersection and goes to cell C4.

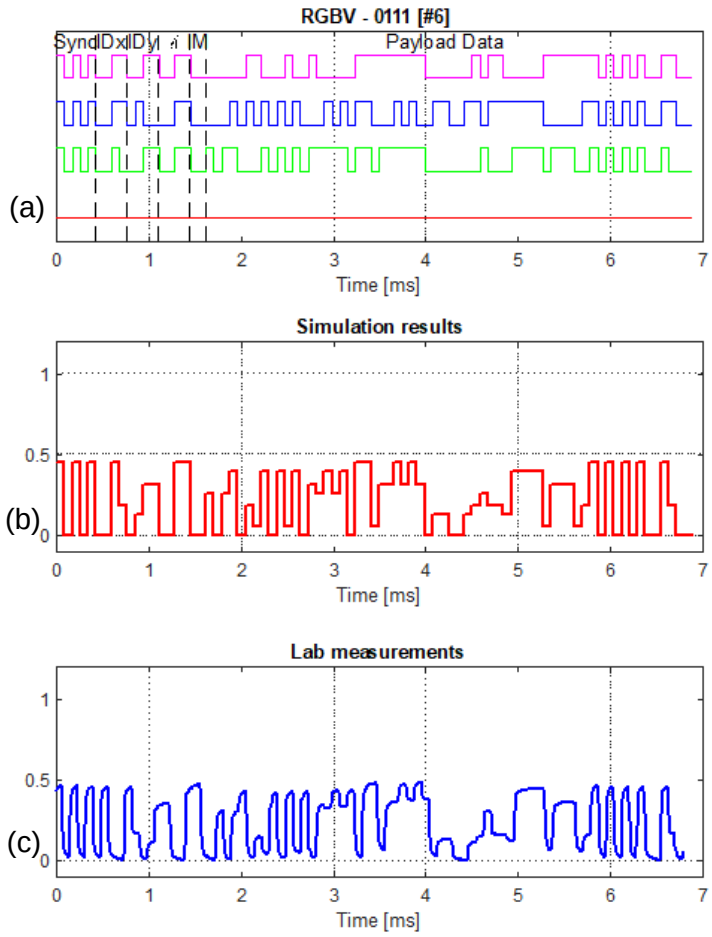

Figure 5.11: Results of the proposed scenario, West to East, cell C4 (position 5), footprint #6: (a) transmitted signals by each channel, (b) simulation of the normalized received signal and (c) normalized experimental received signal.

The signal transmitted by each LED/channel is displayed on the top frame, Figure 5.11 (a). When leaving the intersection and entering cell C4, the vehicle occupies footprint #4.

It is observed that the maximum amplitude of the received signal is again lower than 0.5 due to the absence of the red LED/channel.

Both the simulated and the measured signal are similar. The differences in both received signals are again justified by the capacitive effect of the LED.

This frame, once more, follows the structure presented in Table 4.1. The sync pattern is followed by the ID of the cell ($R_{UNKNOWN}$, $G_{2,3}$, $B_{3,4}$, $V_{3,3}$), the angle (3 or 0º), the IM ([00]) and the payload.

5.4.2 West to North (left turn)

The second scenario is a left turn, from West to North. In Figure 5.12, the vehicle starts in cell C2, before the crossroad, moves forward to cell C3 and turns left. The vehicle ends in cell C1, after leaving the crossroad.

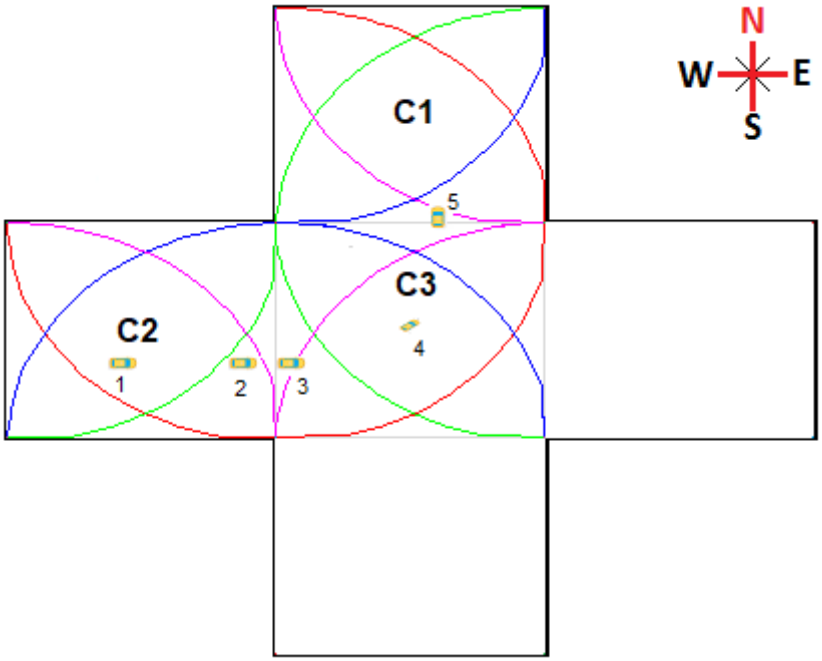

Figure 5.12: Proposed scenario, vehicle moving from West to North.

Figure 5.13 shows the results for cell C2.

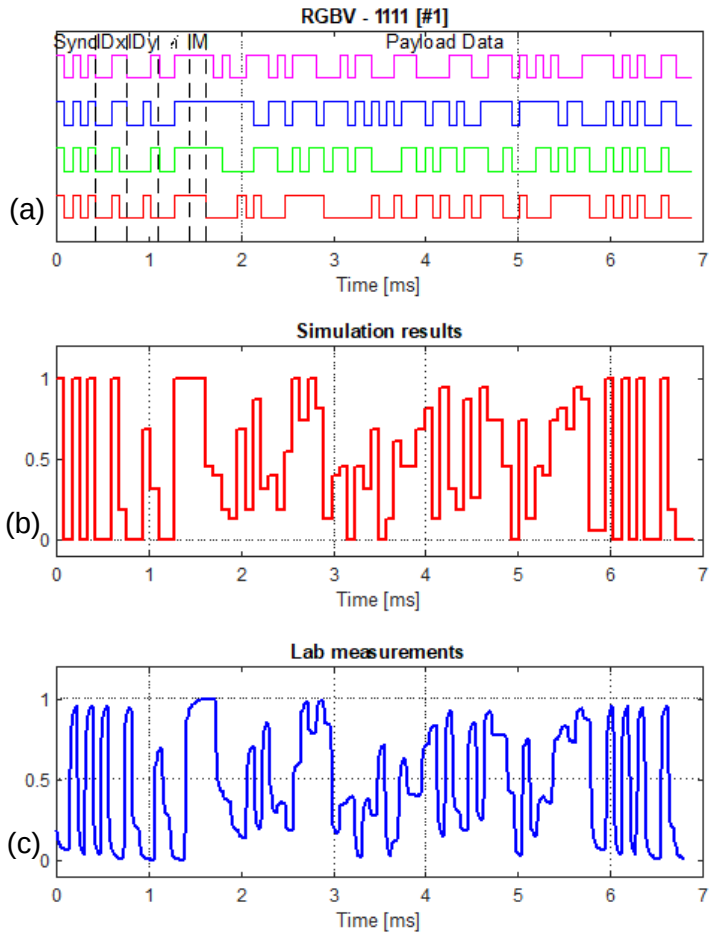

Figure 5.13: Results of the proposed scenario, West to North, cell C2 (position 1), footprint #1: (a) transmitted signals by each channel, (b) normalized simulation of the received signal and (c) normalized experimental received signal.

The signal transmitted by each LED/channel is displayed on the top frame, Figure 5.13 (a). The vehicle at position 1 occupies footprint #1 in cell C2.

The figure structure is the same as in scenario West to East.

As the vehicle is in range of all LED/channels, the maximum amplitude of the signal is one.

Comparing the received signals (middle and bottom frames, Figure 5.13 (b) and (c), respectively) it is possible to conclude that both the simulated and the measured signals are similar, which shows that the simulation tool replicates the laboratory results.

There are few differences, especially when it comes to the two weakest/less intense LED/channels: the blue and violet LED/channels. Their presence or absence is not as noticeable as the others and the capacitive effect of the LED also affects the perceived result.

The frame follows the structure presented in Table 4.1. At the beginning the sync pattern is transmitted followed by the ID of the cell ($R_{2,2}$, $G_{2,1}$, $B_{3,2}$, $V_{3,1}$). The angle is 3 ([0011] in binary) which correspond to zero degrees (0º) and the IM pattern is [11] meaning that this message was transmitted from the IM to the vehicle.

Still in cell C2, the vehicle moves to the next position. The results are displayed in Figure 5.14.

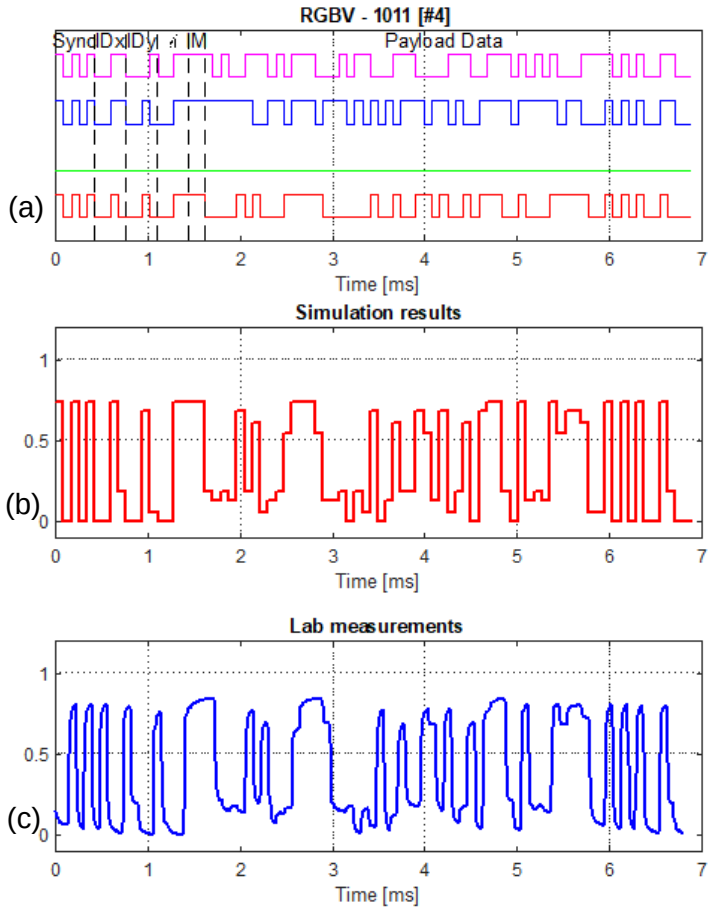

Figure 5.14: Results of the proposed scenario, West to North, cell C2 (position 2), footprint #4: (a) transmitted signals by each channel, (b) normalized simulation of the received signal and (c) normalized experimental received signal.

The signal transmitted by each LED/channel is displayed on the top frame, Figure 5.14 (a). The vehicle at position 2 occupies footprint #4 of cell C2.

As can be seen from Figure 5.14, the maximum amplitude of the received signal is between 0.5 and one, since only the green LED/channel is missing.

By comparing the received signals in Figure 5.14 (b) and (c), it is concluded once again that both the simulated and the measured signals are similar. The few observed differences arise

especially when the blue and violet LED/channels are on, because these are the two less intense LED/channels. Their presence or absence is not as noticeable as the red LED/channel. The capacitive effect of the LED also affects the experimental result.

The frame follows the structure presented in Table 4.1. At the beginning the sync pattern is transmitted, followed by the ID of the cell ($R_{2,2}$, $G_{UNKNOWN}$, $B_{3,2}$, $V_{3,1}$). The angle is 3 ([0011] in binary) which corresponds to zero degrees (0º) and the IM pattern is [11] meaning that this message was transmitted from the IM to the vehicle.

Next, the vehicle leaves cell C2 and enters the crossroad, cell C3 (Figure 5.15).

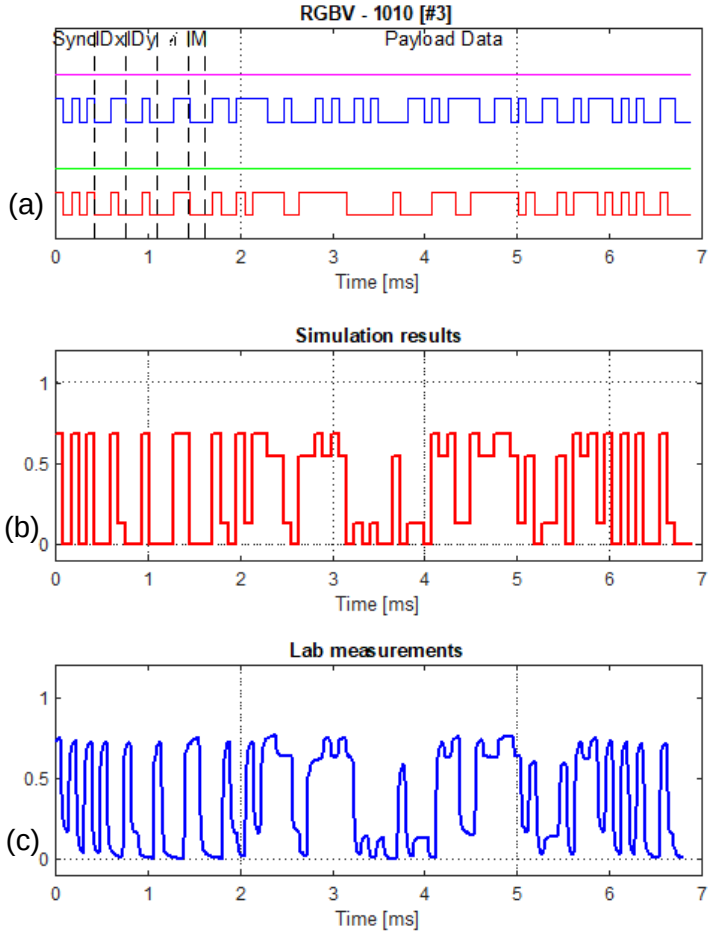

Figure 5.15: Results of the proposed scenario, West to North, cell C3 (position 3), footprint #3: (a) transmitted signals by each channel, (b) normalized simulation of the received signal and (c) normalized experimental received signal.

The signal transmitted by each LED/channel is displayed on the top frame in Figure 5.15 (a). The received signals are displayed in Figure 5.15 (b) and (c) (simulated and measured, respectively). The vehicle at position 3 occupies footprint #3 of cell C3.

The maximum amplitude of the received signal is lower than one, because the green and violet LED/channels are out of range and the signal is over 0.5 due to the presence of red LED/channel.

Comparing the received signals of Figure 5.15 it is possible to conclude that both simulated measured signals are similar. This shows, once again, that the simulation tool can reproduce the results from the laboratory. The observed differences are mainly due to the LED capacitive effects that were not included in the model used for the simulation output.

The frame follows the structure presented in Table 4.1. At the beginning the sync pattern is transmitted, followed by the ID of the cell ($R_{2,2}$, $G_{UNKNOWN}$, $B_{3,2}$, $V_{UNKNOWN}$). The angle is 3 ([0011] in binary) which correspond to zero degrees (0º) and the IM pattern is [00] meaning that this message was transmitted from the vehicle to the IM.

Next, the vehicle turns towards North, still in cell C3 (Figure 5.16).

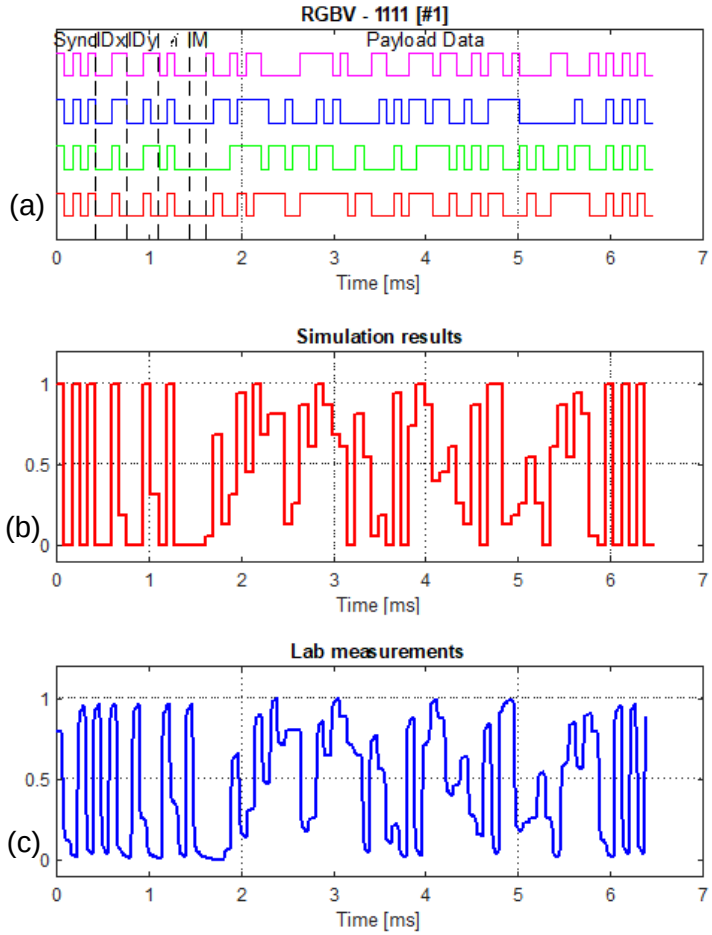

Figure 5.16: Results of the proposed scenario, West to North, cell C3 (position 4), footprint #1: (a) transmitted signals by each channel, (b) normalized simulation of the received signal and (c) normalized experimental received signal.

The vehicle at position 4 occupies the footprint #1 of cell C3.

The maximum amplitude of the received signal is one, because the vehicle occupies footprint #1 receiving the optical signals from the four LED/channels.

Results demonstrate again that the simulation model reproduces accurately the experimental data. Once again, the capacitive effect of the LED affects the perceived result, causing a few differences in both signals.

The frame presented in Figure 5.16 follows the structure presented in Table 4.1. At the beginning the sync pattern is transmitted, followed by the ID of the cell ($R_{2,2}$, $G_{2,3}$, $B_{3,2}$, $V_{3,3}$). At this position the angle changes from 3 to 4 ([0100] in binary) which correspond to 45º since the vehicle is turning left. The IM pattern is [00] meaning that this message was transmitted from the vehicle to the IM.

Lastly, after turning completely left, the vehicle leaves the intersection and moves to cell C1. Results are shown in Figure 5.17.

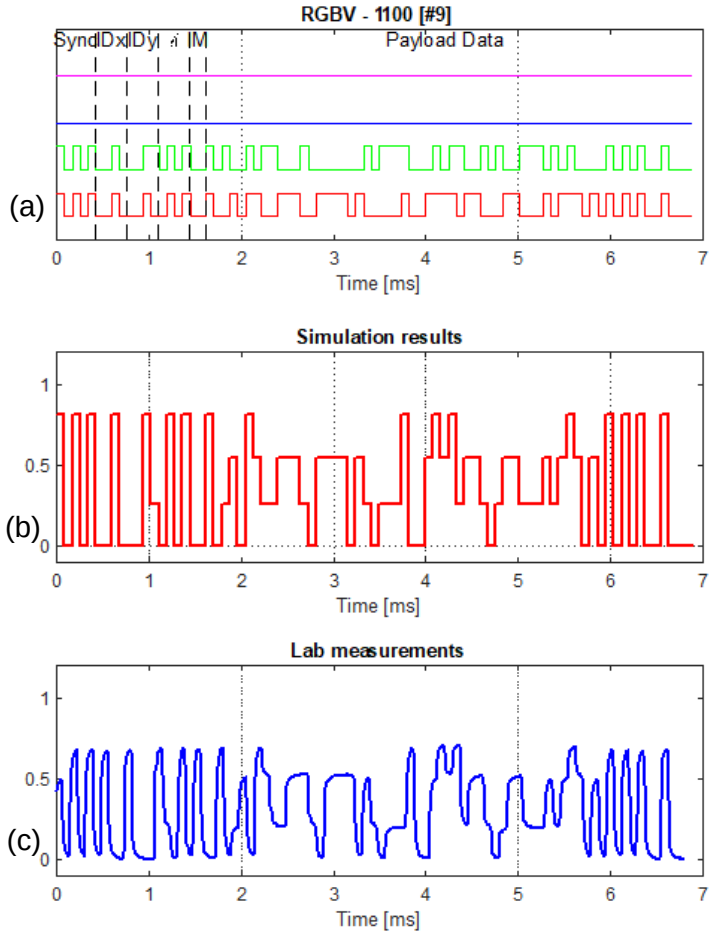

Figure 5.17: Results of the proposed scenario, West to North, cell C1 (position 5), footprint #1: (a) transmitted signals by each channel, (b) normalized simulation of the received signal and (c) normalized experimental received signal.

The vehicle occupies footprint #9 in cell C1.

The maximum amplitude of the received signal is lower than one but over 0.5 because in this position, the vehicle is only in the transmission range of the red and green LED/channels.

There is good agreement between the simulated and the measured. In this footprint, the differences observed between both signals are almost imperceptible, as in this footprint the only active channels are the red and green LED/channels.

The frame in Figure 5.17 follows the structure presented in Table 4.1. At the beginning the sync pattern is transmitted, followed by the ID of the cell ($R_{2,2}$, $G_{2,3}$, $B_{UNKNOWN}$, $V_{UNKNOWN}$). The angle changes to 5 ([0101] in binary) which correspond to 90º since the vehicle is now going

North. The IM pattern is [00] meaning that this message was transmitted from the vehicle to the IM.

5.5 Decoding

The final step of the communication is the decoding process. The goal is to obtain the transmitted signal by each LED/channel from the multiplexed received signal. This ensures that the vehicle and the infrastructure with which it communicates understand one another.

The decoding process starts with the received signal. The vehicle (or infrastructure) uses the calibration curve to match each level of the received signal to the respective LED/channel combination.

As mentioned before in subchapter 4.5, the four LED/channels generates 16 possible combination and each one is associated with a step of the calibration curve. Each step of the signal is compared with the calibration curve and once the match is found, the correspondent combination of the LED/channels is displayed.

5.5.1 Decoding the simulated signal

A few examples of this process are shown in the following figures. The calibration curve used is displayed in Figure 5.3 (a).

The first example is the decoding process where the vehicle is under the transmission range of the four channels (footprint #1). In Figure 5.18 the simulated received signal, the correspondent input coded signals of each channel and the decoded signal are displayed.

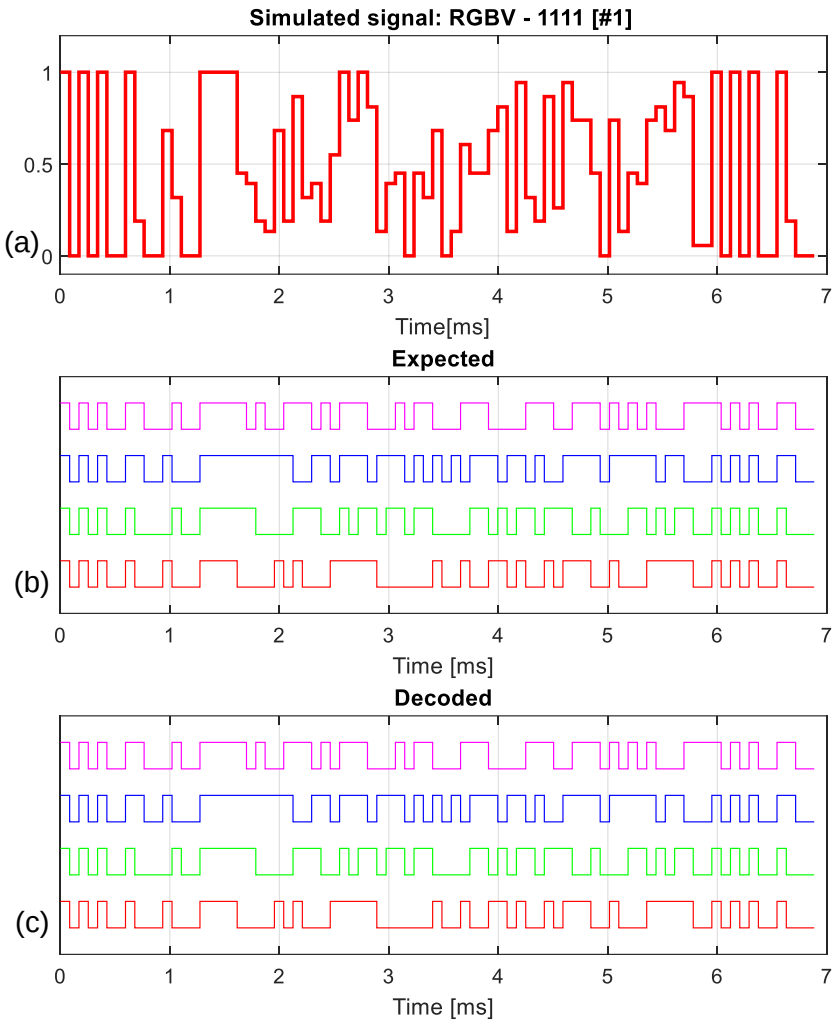

Figure 5.18: Decoded simulated signal, West to North, cell C2 (position 1), footprint #1: (a) received signal, (b) expected decoding result and (c) obtained decoding result.

The top frame (Figure 5.18 (a)) shows the simulation of the multiplexed signal received by the photodetector. The middle frame (Figure 5.18 (b)) shows the transmitted bit sequences by each channel used to produce the multiplexed signal of Figure 5.18 (a). The bottom frame (Figure 5.18 (c)) shows the decoded signals of each input channel using the multiplexed signal (Figure 5.18 (a)) and the calibration curve (Figure 5.3 (a)). In footprint #1 all LED/channels are in the range and the maximum amplitude of the received signal is equal to one.

The comparison of the transmitted/expected and decoded signals displayed shows that the decoding process was fully successful as there is a complete match of every single bit of the transmitted frame by every channel.

The following results (Figure 5.19) show the decoding process where the user is in the range of only three LED/channels.

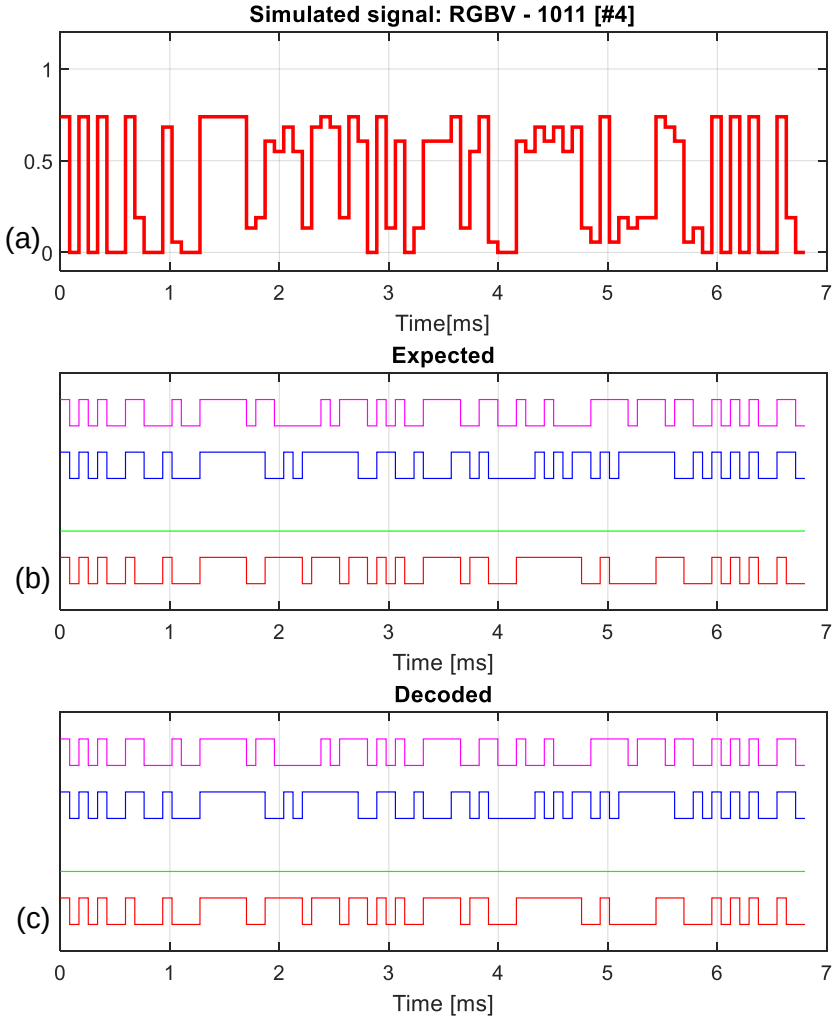

Figure 5.19: Decoded simulated signal, West to East, cell C2 (position 1), footprint #4: (a) received signal, (b) expected decoding result and (c) obtained decoding result.

Figure 5.19 (a) shows the received signal to be decoded, in the middle and bottom frames the expected and decoded signals respectively (Figure 5.19 (b) and (c)). In footprint #4 the green LED/channel is out of range and the maximum amplitude of the received signal is between 0.5 and one.

As seen in Figure 5.19, the decoding process succeeded. Every LED/channel matches the expected result.

Figure 5.20 shows the decoding process where only two LED/channels are in range.

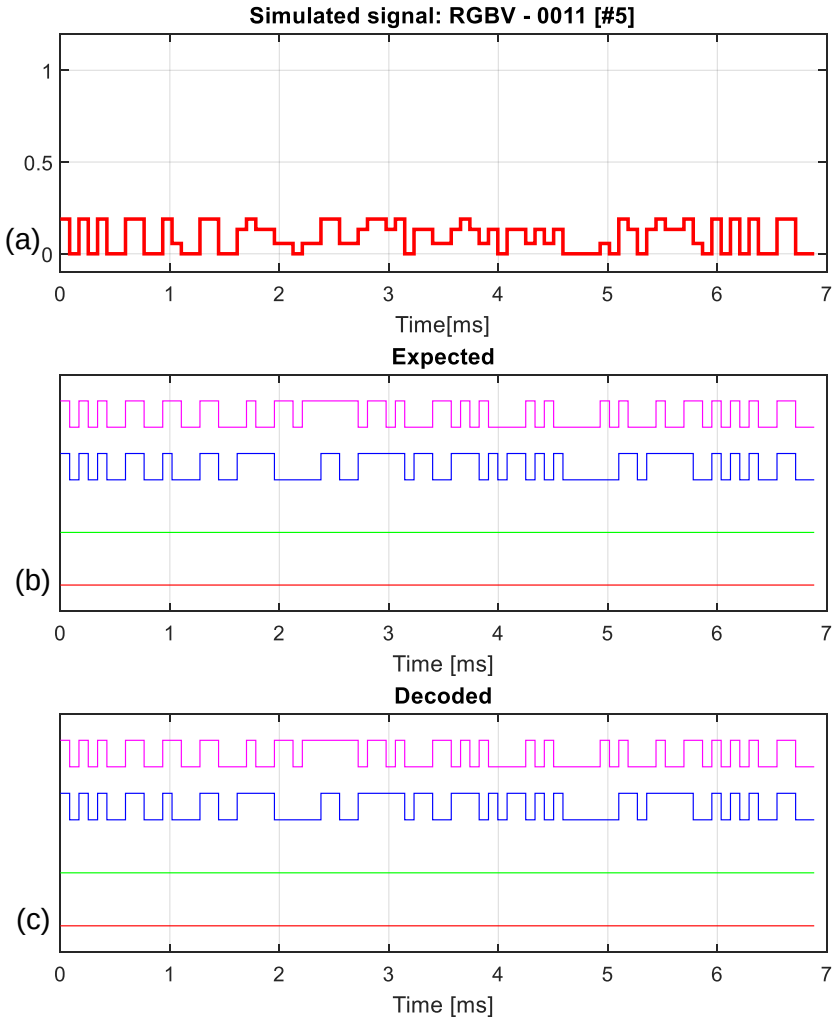

Figure 5.20: Decoded simulated signal, West to East, cell C3 (position 3), footprint #5: (a) received signal, (b) expected decoding result and (c) obtained decoding result.

Figure 5.20 (a) shows the received signal to be decoded and Figure 5.20 (b) and (c) shows the expected and decoded signals respectively. In footprint #5 the red and green LED/channel are out of range and the maximum amplitude of the received signal is lower than 0.5.

As seen in Figure 5.20, the decoding process succeeded. Every LED/channel matches the expected result.

5.5.2 Decoding the measured signal

The implementation of the decoding algorithm for the simulated signals proved to be very efficient with a full match of every bit of each frame for all channels, independently on the number of channels covered by the user's range. The second part of the decoding task was done using the experimental data instead of the simulated data.

A few examples of this process are shown in the following figures. The calibration curve used is displayed in Figure 5.3 (b).

The first example is the decoding process where all the LED/channels are in range (footprint #1), Figure 5.21.

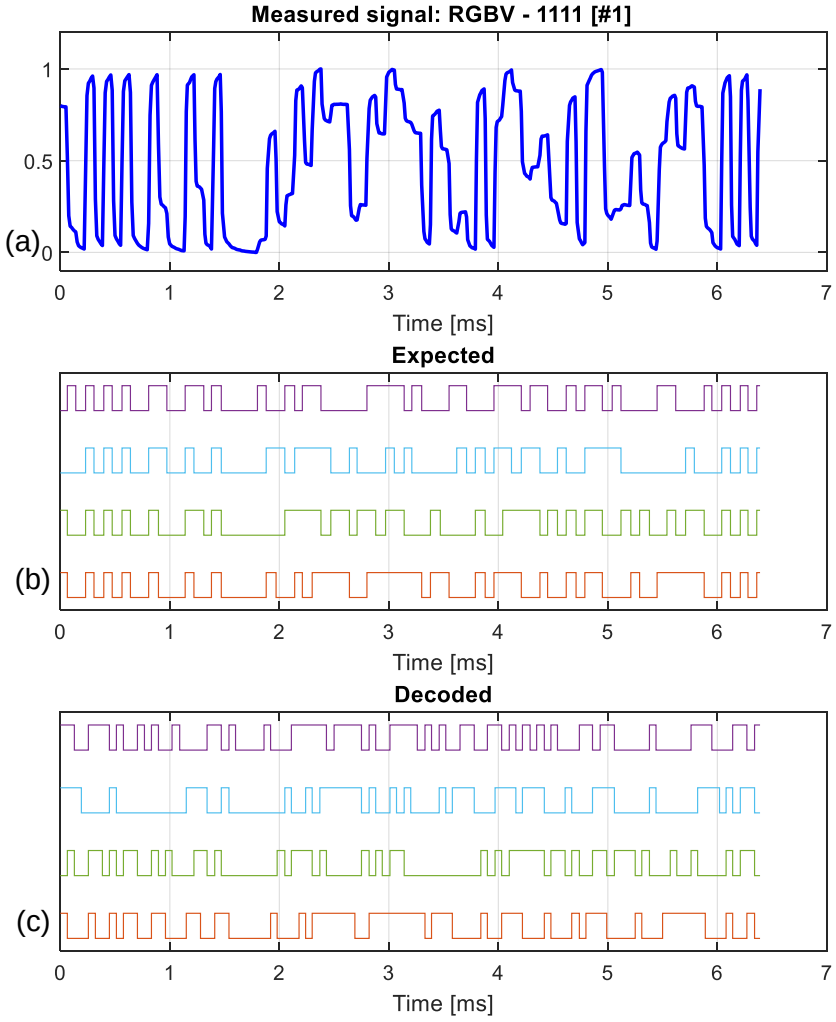

Figure 5.21: Decoded measured signal, West to North, cell C3 (position 4), footprint #1: (a) received signal, (b) expected decoding result and (c) obtained decoding result.

In footprint #1 all LED/channels are in range and the maximum amplitude of the received signal one.

As seen in Figure 5.21, the decoding process for lab measurements is not as successful as for the simulated. The result differs slightly from the expected. The red LED/channel is the closest to the expected result. This is because this LED/channel is more intense than the others which makes it more distinguishable. The signal levels from the blue and violet LED/channel are less distinguishable (as seen in Figure 5.3 (b)) making the decoding process less precise.

A solution for this decoding problem is providing a more distinguishable calibration curve and/or implementing error correction through parity (explained in subchapter 3.1). Another possible solution is implementing a mechanism to detect and correct the size of each bit in the measured signal. Occasionally, the program used to obtain the measured signal changes the number of samples in each bit and the received signal used for the decoding process is affected. Because of this and given that the decoding process uses an average value for bit size, some bits are decoded incorrectly. The error is carried throughout the entire frame.

Figure 5.22 shows the decoding process where three LED/channels are in range.

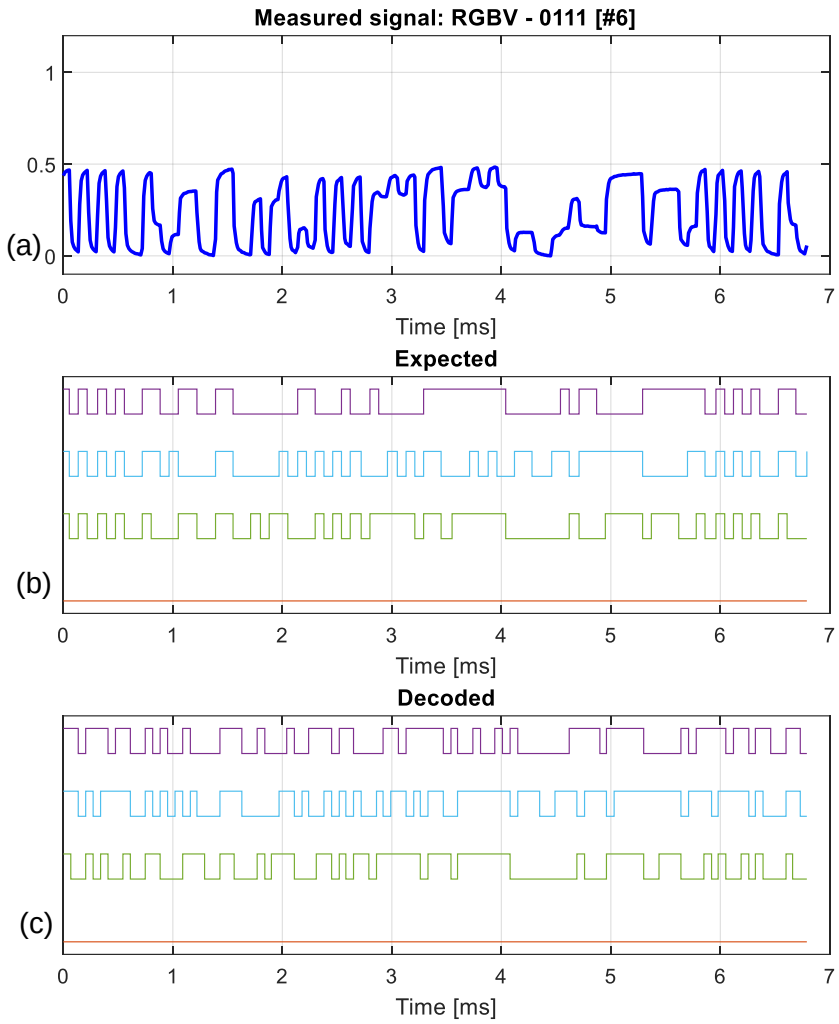

Figure 5.22: Decoded measured signal, West to North, cell C4 (position 5), footprint #6: (a) received signal, (b) expected decoding result and (c) obtained decoding result.

In footprint #6 the red LED/channel is out of range and the maximum amplitude of the received signal is lower than 0.5.

As seen in Figure 5.22, the decoding process presents a few errors and the result differs slightly from the expected. The red LED/channel is exactly as expected due to it being more intense than the others which makes it more distinguishable, and the green is very close to the expected result. However, the blue and violet LED/channel were not correctly decoded.

Once again, the solution for the decoding problem could be providing a more distinguishable calibration curve and/or implementing error correction through parity check bits (explained in subchapter 3.1). Additionally, decoding inaccuracies can also be corrected by implementing a mechanism to detect and correct the size of the bits. As the decoding process uses an average

value for bit size and because the received signal is already affected by the occasional change in number of samples for each bit, the error is carried throughout the frame.

Figure 5.23 shows the decoding process where only two LED/channels are in range.

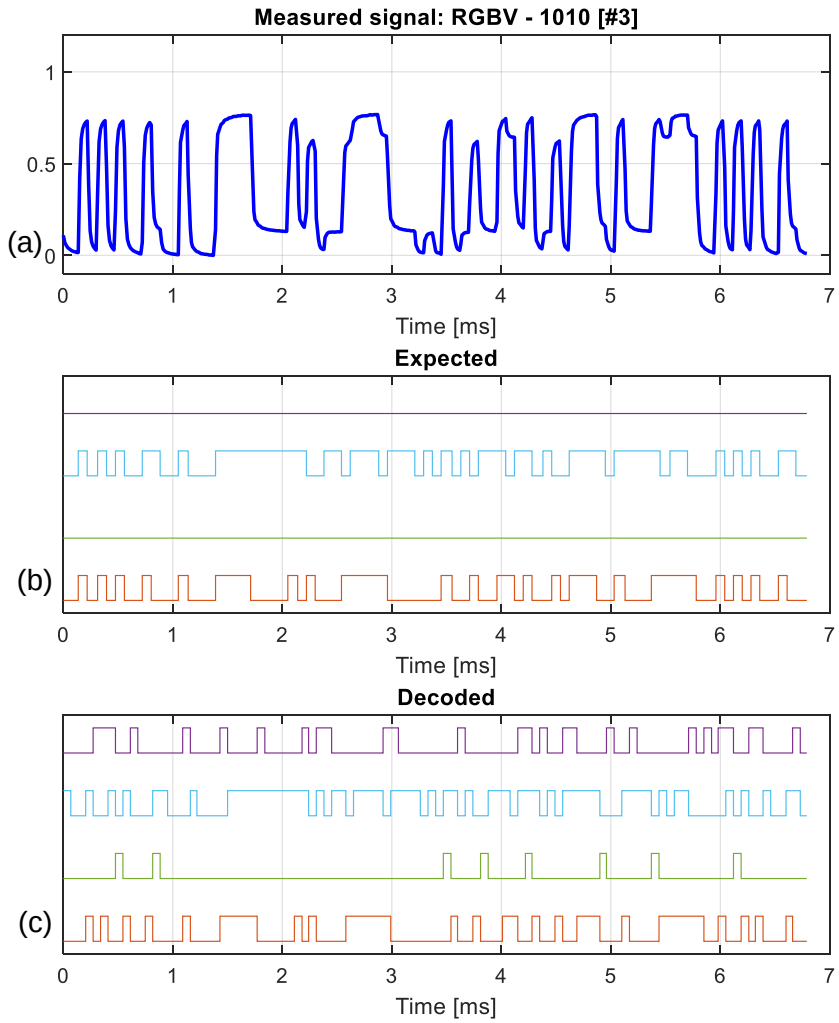

Figure 5.23: Decoded measured signal, West to North, cell C3 (position 3), footprint #3: (a) received signal, (b) expected decoding result and (c) obtained decoding result.

In footprint #3 the green and violet LED/channel are out of range and the maximum amplitude of the received signal is lower than one.

Once again, the red LED/channel was nearly perfectly decoded, and the green LED/channel presents a few errors. The blue and violet LED/channel still presents the most errors in the decoding process which can be resolved with parity implementation (explained in subchapter

3.1). Since experimental sampling does not always result in bits of the same size, the decoding process undergoes an additional source of noise. Detecting and correcting the bit size can be another method for fixing decoding errors.

5.6 Graphical User Interface

A Graphical User Interface, GUI, composed of three tabs was developed. The GUI helps the user to interact with the simulation tool in an easier way and provides all the functionalities for simulation and data analysis.

In Figure 5.24 the first tab “Proposed Scenario” is displayed. Here, it is possible to visualize the proposed scenario (five cell crossroad) by pressing the button “Crossroad”. The user has the possibility of choosing the intensity, IN, the wavelength, λ, of each LED/channel, and the channel/receiver gain, Gain R, and, after running the scenario, displaying the coverage and footprint maps.

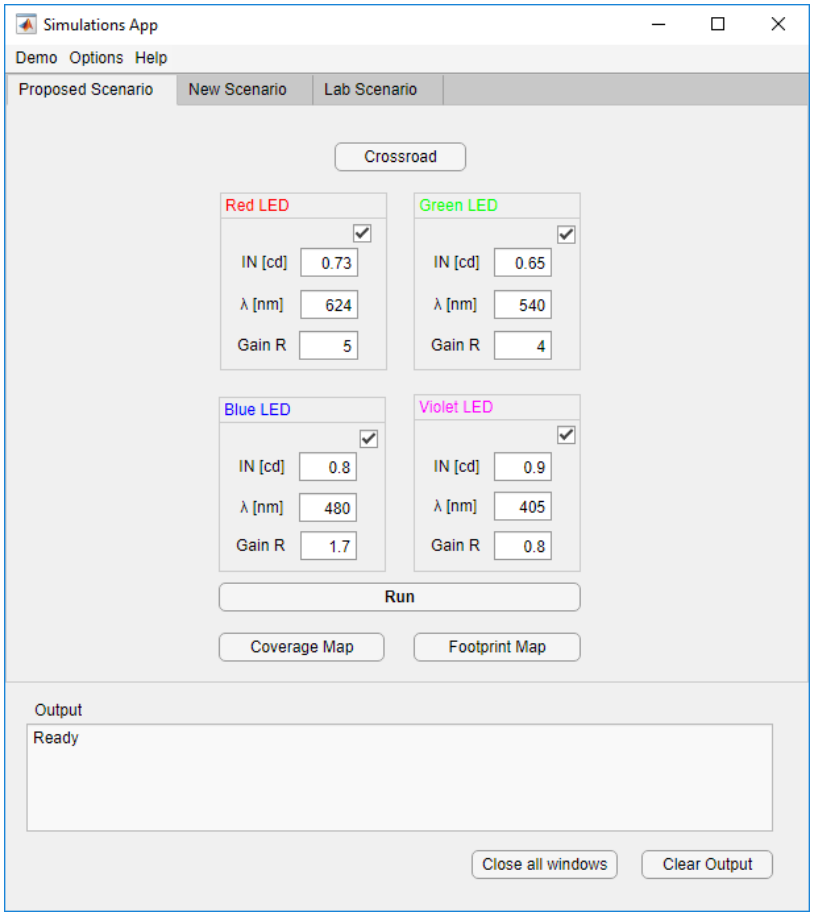

Figure 5.24: Graphical User Interface, tab one.

The second tab is displayed in Figure 5.25. After running the scenario in tab one, the user can display the calibration curve, the frame, and the decoded frame by pressing the “Calibration”, “Frame”, and “Decode” buttons, respectively. The ID, Angle and IM can be inserted by the user. The payload can either be inserted by the user or generated randomly by checking the “Random Payload (50 bits)” box. The ID can be found in the “Crossroad” button in the first tab and the Angle can be found in “Pose Orientation” button in the second tab.

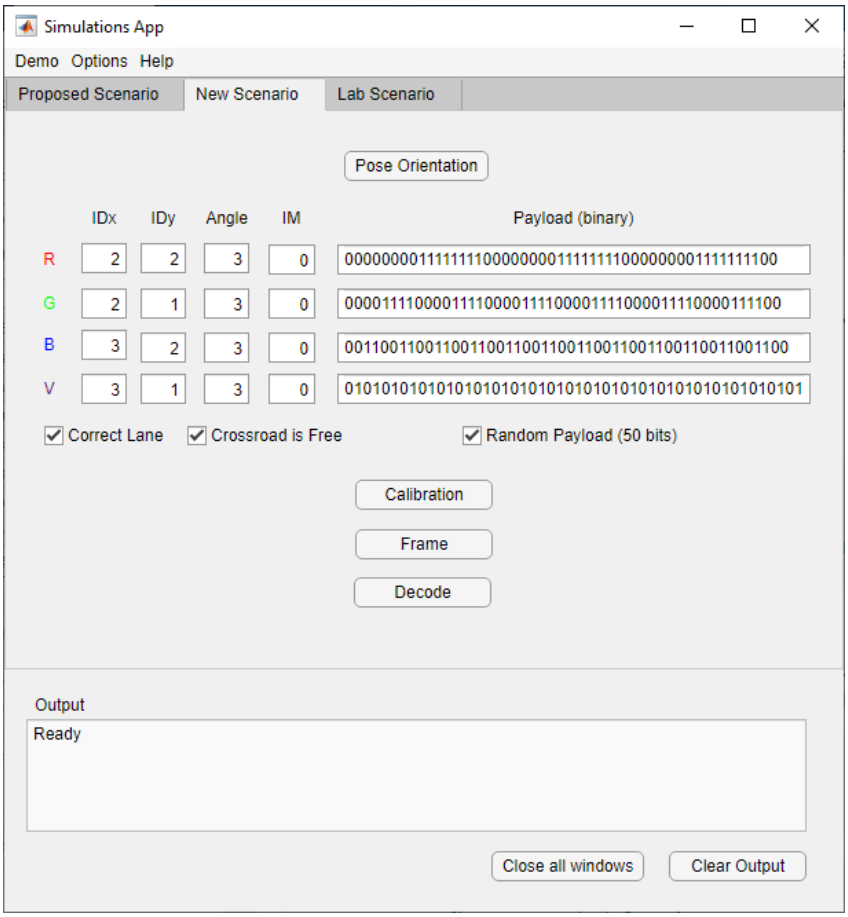

Figure 5.25: Graphical User Interface, tab two.

In subchapter 5.4 it was assumed that all vehicles were granted permission to cross the intersection and that the lane occupation was correct. But this is not always the case. The intersection manager is responsible to ensure a safe crossing of the intersection, making sure that the vehicle is occupying the correct lane for the intended direction and that it is safe to cross the intersection, avoiding collision.

This was implemented with two checkboxes, “Correct Lane” and “Crossroad is Free”. Access to the crossroad is denied if the second checkbox (“Crossroad is free”) is not selected. On the other hand, if it is selected, access to the crossroad is granted. The first checkbox (“Correct Lane”) verifies if the vehicle’s intended route is viable, meaning that if the vehicle needs to turn left, the correct lane is the left one. For straight route or right turn, the correct lane is the right

lane. By selecting the first checkbox, it is assumed that the vehicle is occupying the correct lane for its intention.

Finally, the third tab is displayed in Figure 5.26. This is where the user can view the laboratory measurements by specifying the .xlsx file and the calibration and frame sheets. The calibration curve is viewed by pressing the “Calibration” button, the frame is viewed by pressing the “Frame” button and the decoded frame can be viewed by pressing the “Decode” button.

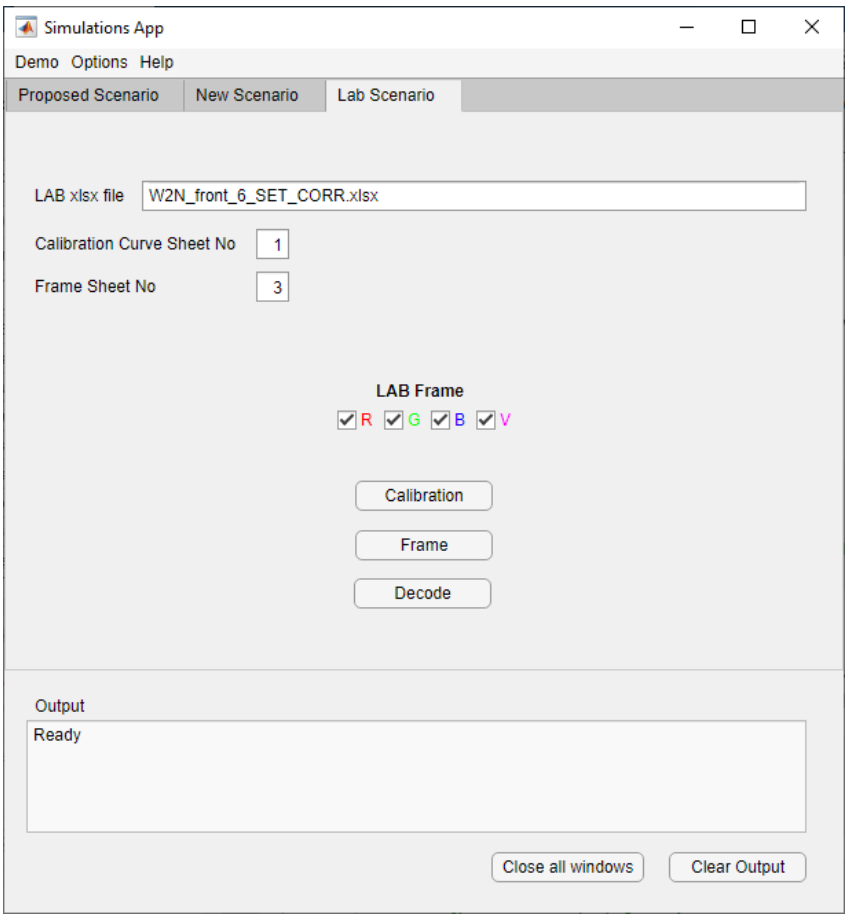

Figure 5.26: Graphical User Interface, tab three.

On the bottom of the window, a “Status” panel displays messages when each action is finished. For the second frame in Figure 5.25, depending if the “Correct Lane” or the “Crossroad is Free” boxes are checked, a message giving or denied access to the crossroad is also displayed.

It is possible to verify the scenarios presented in chapter 5 on the top of the window in the “Demo” menu. In the “Options” menu the user can restart and close the application. In the “Help” menu, the user can access the instructions and the parameter legend.

6 Conclusion and Future Work

The theoretical study of the subject, VLC, the analysis of proposed methodologies and the development of the simulation program were crucial steps in the development and writing of this dissertation.

After deep study of the VLC technology, it was possible to realize the main features of this technology and its attractiveness as an optical wireless technology. The use of LEDs as lighting solutions is becoming very popular due to its high efficiency and good performance that favored the launch of the VLC technology.

Since it is a technology based on visible light, and the spectrum is practically untouched for communication, it is a great alternative to the RF technology. By applying VLC in vehicular communication, road safety can the improved.

As any other technology, VLC faces many challenges. In outdoor scenarios, the major challenge is related to noise caused by various sources of light (both artificial and natural), as well as multiple reflections.

The proposed test scenario intends to provide better security and throughput of a traffic intersection. Vehicles and infrastructures are equipped with transmitters and receivers to communicate with each other using V2I, I2V or V2V communication links.

A white light source composed of a tetrachromatic LED with a single modulated channel is proposed to transmit data. The other three channels of the white LED are used only for illumination.

Each LED is located at a corner of the intersection forming a grid adjusted to avoid overlap of adjacent grid points. The overlap of the transmission range of each LED of a cell is called a footprint. Four LEDs generate nine possible footprints labelled from 1 to 9. Footprint 1 corresponds to the overlap of all four LEDs, footprints with even labels (2, 4, 6 and 8) correspond to the overlap of three LEDs and odd labeled footprints (3, 5, 7 and 9) correspond to the overlap of two LEDs.

The OOK modulation and the transmission scheme was based on a 64-bit codification.

The model uses the luminous intensity of the LED as the emitted power. The pathloss is modeled based on the distance between transmitter and receiver, and the wavelength of each channel. Initially, the 3GPP antenna model was used. However, it was replaced with the Lambertian model which is more suitable for the LED used as optical light source. All these parameters are necessary when calculating the link budget, which is used to obtain the

coverage map. The message is encoded using a 64-bit frame structure and decoded at the receiver unit.

The coverage map can be used to predict the receiver's power at each point on the map and the footprint map can be used to observe the LED's transmission range at each point on the map.

The calibration curve is used to support the decoding process at the receiver unit. During the calibration process, a value was assigned to each of the 16 levels of the curve allowing them to be identified as input of the optical channel

To verify the simulation tool, two scenarios were tested and measured in the laboratory: vehicle moving from West to East and from West to North.

The simulated encoded message matched the measured encoded message, proving that the used encoding method generates valid results. For each footprint of the analyzed trajectories, the multiplexed signal at the photodetector was measured experimentally in the laboratory and compared with the one simulated with the developed model. The footprint affects the maximum amplitude of the signal. If the red LED/channel is present, the maximum signal amplitude is usually over 0.5 and if all the LED/channels are present the maximum amplitude is one. Similarities where blue and violet LED/channels are present were noted due to these being the less intense signals. The capacitive effect of the LED is also a reason for said similarities.

The decoding process was fully successful with the simulated multiplexed signals. This was not the case with the laboratory measurements, as a few errors were detected. Generally, the red LED/channel presents the least errors since it is more intense than the other ones, so it is easier to distinguish and less prone to decoding errors. The green is usually the second LED/channel with the least errors. The blue and violet LED/channels are less distinguishable, as seen in the calibration curve, making the calibration process less precise and leading to more errors.

A possible solution to decrease the errors in the decoding process of the laboratory measurements could be adjusting the calibration curve to improve the distinction of each level or implementing an error detection mechanism such as the parity check bits. In addition, the size of the samples of each bit of the measured signal also affects the decoding process. Mitigation of this effect would benefit the decoding process.

A GUI was developed to enable easy interaction between the user and the simulation tool.

The program used for simulations was developed in MATLAB. The program reads a BMP file containing information about the positioning of each LED. The emitted power, the

receiver/channel gain, and the wavelength are input values to calculate the pathloss and consequently providing outputs such as the coverage map, the footprint map, and the calibration curve.

Future developments can be made to this dissertation. A few immediate improvements to the developed work include the modelling of the multiplexed signal using the capacitive effects of the LED and the detection and correction of the number of samples of each bit. Furthermore, the improvement of the decoding mechanism is an urgent task that can be done either by adjusting the calibration curve to improve the distinction of each level or by using parity check bits as error control and correction. In a broader context, future work could also involve developing models for NLOS scenarios, using other modulations, and scaling up the prototype model.

References

[1] L. Teixeira, F. Loose, J. P. Brum, C. H. Barriquello, V. A. Reguera and M. A. D. Costa, "On the LED Illumination and Communication Design Space for Visible Light Communication," *IEEE Transactions on Industry Applications,* vol. 55, no. 3, pp. 3264-3273, May-June 2019, doi: 10.1109/TIA.2019.2900209.

[2] P. H. Pathak, X. Feng, P. Hu and P. Mohapatra, "Visible Light Communication, Network and Sensing: A Survey, Potential and Challenges," *IEEE Communications Surveys & Tutorials,* vol. 17, no. 4, pp. 2047-2077, Fourthquarter 2015, doi: 10.1109/COMST.2015.2476474.

[3] N. Kumar and N. R. Lourenço, "Led-Based Visible Light Communication System: A Brief Survey and Investigation," *Journal of Engineering and Applied Science,* vol. 5, no. 4, pp. 296-307, 2010.

[4] K. Lee, H. Park and J. R. Barry, "Indoor Channel Characteristics for Visible Light Communications," *IEEE Communications Letters,* vol. 15, no. 2, pp. 217-219, Feb. 2011.

[5] S. Arnon, Visible Light Communication, Cambridge University Press, 2015.

[6] H. Haas, L. Yin, Y. Wang and C. Chen, "What is LiFi?," *Jounar of Lightwave Technology,* vol. 34, no. 6, pp. 153-1544, 2016.

[7] Y. Qiu, H.-H. Chen and W.-X. Meng, "Channel Modeling for Visible Light Communication - a Survey," *Wireless Communications and Mobile Computing,* pp. 2016-2034, 2016, doi: 10.1002/wcm.2665.

[8] G. A. Mapunda, R. Ramogomana, L. Marata, B. Basutli, A. S. Khan and J. M. Chuma, "Indoor Visible Light Communication: A Tutorial and Survey," *Wireless Communications and Mobile Computing,* Vol. 2020, Article ID 8881305, 46 pages, https://doi.org/10.1155/2020/8881305.

[9] H. Haas, J. Elmirghani and I. White, "Optical Wireless Communication," *Philosophical Transactions. Series A, Mathematical, Physical and Engineering Science. 378: 20200051,* http://dx.doi.org/10.1098/rsta.2020.0051.

[10] M. A. Vieira, M. Vieira, P. Louro and P. Vieira, "Redesign of the Trajectory Within a Complex Intersection for Visible Light Communication Ready Connected Cars," *Society*

of Photo-Optical Instrumentation Engineers (SPIE), 2020, doi: 10.1117/1.OE.59.9.097104.

[11] M. A. Vieira, M. Vieira, P. Louro, M. de Lima and P. Vieira, "Vehicular Visible Light Communication in a Two-Way-Two-Way Traffic Light Controlled Crossroad," in *SENSORDEVICES 2021*, Atenas, November 14-18, 2021.

[12] A.-M. Căilean and M. Dimian, "Current Challenges for Visible Light Communications Usage in Vehicle Applications: A Survey," *IEEE Communications Surveys & Tutorials,* vol. 19, no. 4, pp. 2681-2703, Fourthquarter 2017, doi: 10.1109/COMST.2017.2706940.

[13] L. Cheng, W. Viriyasitavat, M. Boban and H.-M. Tsai, "Compatison of Radio Frequency and Visible Light Propagation Channels for Vehicular Communications," *IEEE Access,* vol. 6, pp. 2634-2644, 2018, doi: 10.1109/ACCESS.2017.2784620.

[14] X. Li, R. Zhang and L. Hanzo, "Optimization of Visible-Light Optical Wireless Systems: Network-Centric Versus User-Centric Designs," *IEEE Communications Surveys & Tutorials,* vol. 20, no. 3, pp. 1878-1904, thirdquarter 2018, doi: 10.1109/COMST.2018.2813433.

[15] M. Kashef, M. Ismail, M. Abdallah, K. A. Qaraqe and E. Serpedin, "Energy Efficient Resource Allocation for Mixed RF/VLC Heterogeneous Wireless Networks," *IEEE Journal on Selected Areas in Communications,* vol. 34, no. 4, pp. 883-893, April 2016, doi: 10.1109/JSAC.2016.2544618.

[16] P. Louro, M. Vieira, M. A. Vieira, M. de Lima, J. Rodrigues and P. Vieira, "Footprint Model in a Navigation System Based on Visible Light Communication," *SENSORDEVICES 2021,* Atenas, 14-19 November 2021.

[17] T. Komine and M. Nakagawa, "Fundamental Analysis for Visible-Light Communication System using LED Lights," *IEEE Transactions on Consumer Electronics,* vol. 50, no. 1, pp. 100-107, Feb. 2004, doi: 10.1109/TCE.2004.1277847.

[18] H. Elgala, R. Mesleh and H. Haas, "Indoor Optical Wireless Communication: Potential and State-of-the-Art," *IEEE Communications Magazine,* vol. 49, no. 9, pp. 56-62, 2011, doi:10.1109/MCOM.2011.6011734.

[19] H. Q. Nguyen, J.-H. Choi, M. Kang, Z. Ghassemlooy, D. H. Kim, S.-K. Lim, T.-G. Kang and C. G. Lee, "A MATLAB-based Simulation Program for Indoor Visible Light Communication System," *2010 7th International Symposium on Communication*

Systems, Networks & Digital Signal Processing (CSNDSP 2010), pp. 537-541, 2010, doi: 10.1109/CSNDSP16145.2010.5580355.

[20] M. Z. Chowdhury, M. T. Hossan, A. Islam and Y. M. Jang, "A Comparative Survey of Optical Wireless Technologies: Architecture and Applocations," *IEEE Access,* vol. 6, pp. 9819-9840, 2018, doi: 10.1109/ACCESS.2018.2792419.

[21] A. Memedi and F. Dressler, "Vehicular Visible Light Communications: A Survey," *IEEE Communications Surveys & Tutorials,* vol. 23, no. 1, pp. 161-181, Firstquarter 2021, doi: 10.1109/COMST.2020.3034224.

[22] F. A. Dahri, H. B. Mangrio, A. Baqai and F. A. Umrani, "Experimental Evaluation of Intelligent Transport System with VLC Vehicle-to-Vehicle Communication," *Wireless Pers Commun 106,* pp. 1885-1896, 2019, https://doi.org/10.1007/s11277-018-5727-0.

[23] S. Yu, O. Shih, H. Tsai, N. Wisitpongphan and R. D. Roberts, "Smart Automotive Lighting for Vehicle Safety," *IEEE Communications Magazine,* vol. 51, no. 12, pp. 50-59, December 2013, doi: 10.1109/MCOM.2013.6685757.

[24] S. Lee, J. K. Kwon, S.-Y. Jung and Y.-H. Kwon, "Evaluation of Visible Light Communication Channel Delay Profiles for Automotive Applications," *EURASIP J. Wireless Com. Network,* 2012, https://doi.org/10.1186/1687-1499-2012-370.

[25] N. Lourenço, D. Terra, N. Kumar, L. N. Alves and R. L. Aguiar, "Visible Light Communication System for Outdoor Applications," *2012 8th Internatinal Symposium on Communication Systems, Networks & Digital Signal Processing (CSNDSP), Poznan,* pp. 1-6, 2012, doi: 10.1109/CSNDSP.2012.6292744.

[26] B. Soner and S. Coleri, "Visible Light Communication Based Vehicle Localization for Collision Avoidance and Platooning," *IEEE Transactions on Vehicular Technology,* vol. 70, no. 3, pp. 2167-2180, 2021, doi: 10.1109/TVT.2021.3061512.

[27] K. Shaaban, M. H. M. Shamim and K. Abdur-Rouf, "Visible Light Communication for Intelligent Transportation Systems: A Review of the Latest Technologies," *Journal of Traffic and Transportation Engineering (English Edition),* vol. 8, no. 4, pp. 483-492, 2021, https://doi.org/10.1016/j.jtte.2021.04.005.

[28] A. Cailean, B. Cagneau, L. Chassagne, S. Topsu, Y. Alayli and J. Blosseville, "Visible Light Communications: Application to Cooperation Between Vehicles and Road

Infrastructures," *2012 IEEE Intelligent Vehicles Symposium,* pp. 1055-1059, 2012, doi: 10.1109/IVS.2012.6232225.

[29] Cree, *Datasheet: PLCC4 3-in-1 SMD LED CLV1A-FKB,* 2014.

[30] I. Raza, S. Jabeen, S. R. Chaudhry, S. A. Hussain, A. Saeed, M. S. Bhatti and M. H. Raza, "Optical Wireless Channel Characterization For Indoor Visible Light Communications," *Indian Journal of Science and Technology,* vol. 8 (22), September 2015, doi: 10.17485/ijst/2015/v8i22/70605.

[31] "5G; Study on Channel Model for Frequencies from 0.5 to 100 GHz (3GPP TR 38.901 version 16.1.0 Release 16)," *ETSI TR 138 901 V16.1.0,* November 2020.

[32] P. Louro, M. Vieira, P. Vieira, J. Rodrigues and M. de Lima, "Geo-Localization Using Indoor Visible Light Communication," *Proc. SPIE 11772, Optical Sensors 2021,* 117720J (18 April 2021), doi: 10.1117/12.2589477 (conference SPIE Europe 2021, digital forum).

[33] M. A. Vieira, M. Vieira, P. Louro and P. Vieira, "Vehicular Visible Light Communication in a Traffic Controlled Intersection," *Society of Photo-Optical Instrumentation Engineers (SPIE),* 2021.

[34] P. Louro, M. Vieira, M. A. Vieira, M. Fernandes and J. Costa, "Use of a-SiC:H Photodiodes in Optical Communications Applications," in *Advances in Photodiodes*, 2011, pp. 377-401, doi: 10.5772/14048.

[35] M. Vieira, P. Louro, M. Fernandes, M. A. Vieira, A. Fantoni and J. Costa, "Three Transducers Embedded into One Single SiC Photodetector: LSP Direct Image Sensor, Optical Amplifier and Demux Device," in *Advances in Photodiodes*, 2011, pp. 403-425, doi: 10.5772/14098.